Canada

Communications Research Centre

DAMPING SYNTHESIS FOR A SPACECRAFT USING SUBSTRUCTURE AND COMPONENT DATA

by

K.W. LIPS AND F.R. VIGNERON

CRC REPORT NO. 1365

overnment of Canada
epartment of Communications

Gouvernement du Canada
Ministère des Communications

OTTAWA, AUGUST 1984

COMMUNICATIONS RESEARCH CENTRE

DEPARTMENT OF COMMUNICATIONS
CANADA

DAMPING SYNTHESIS FOR A SPACECRAFT USING SUBSTRUCTURE AND COMPONENT DATA

by

K.W. Lips and F.R. Vigneron

(Space Technology and Applications Branch)

CRC REPORT NO. 1365

August 1984
OTTAWA

ABSTRACT

This report demonstrates a method for the synthesis of modal damping factors and other modal data for a spacecraft in orbit, based on input information at the component/substructure level. Also, it illustrates the use of the method and the level of accuracy obtained, in a case study of the Hermes spacecraft.

The synthesis procedure is demonstrated for a spacecraft configuration consisting of a central rigid body, solar array substructures, a momentum wheel and a liquid mercury damping device. The synthesized spacecraft modal data is obtained by eigenproblem analysis of a system model that is constructed from submodels of the components. The system modes are the natural (unconstrained) modes with damping and gyroscopic stiffness accounted for. Numerical experiments show that the procedure is not sensitive to errors in or to omission of damping factors of the higher order substructure modes that are not generally available from test data. Damping factors for the nutational mode are confirmed by an independent analysis based on the Method of Averaging.

In the application of the procedure with Hermes data, the synthesized modal damping factors for the structural modes are found to differ relative to values measured in-orbit by factors ranging from zero to five. The liquid mercury damper is found to be

relatively unimportant, although it could have contributed to damping of the nutational mode if the fluid were excited at resonance. Some of the shortcomings in correlation between synthesized and measured damping factors are believed to be due to inadequacies in the law chosen to model the damping of the solar array, and others to unidentifiable sources of damping such as friction between substructure joints.

TABLE OF CONTENTS

LIST OF TABLES

LIST OF FIGURES

NOMENCLATURE

a_0	distance measured from boom centerline to tip pallet center of mass, Figure 4
a_{11}, a_{12}, a_{21}	coefficients identifying first order behaviour of A(t), B(t); Equations (A.10) - (A.12)
A(t), B(t)	transformed equivalents for $\omega_1(t)$, $\omega_3(t)$; Equations (A.3)
[A]	a coefficient matrix for the coupled first order roll/yaw or pitch system, Equation (14c) or (18b)
b, b^1	width and effective width of array blanket, Table 2
[B]	a coefficient matrix for coupled first order roll/yaw or pitch system, Equation (14d) or (17d)
$\{B_1\}$, $\{B_3\}$	integral over a single array for first moment of in-plane and out-of-plane mode shapes, respectively; Equations (12c)
c_D	linear viscous damping coefficient for damper
{C}	a matrix component of the first order pitch dynamics, Equation (17e)
$\{C_\varepsilon\}$	damping matrix associated with generalized coordinates ε = U,W or $\bar{\alpha}$; Equations (5c)
$\underline{d}$	offset for equilibrium point of damper center of mass measured with respect to '0', having components $d_1 \underline{1}$ + d_2 $\underline{2}$ + 0 $\underline{3}$; Figure 1(c)
dm_i	elemental mass for ith appendage
D	coefficient as defined by Equation (A.9a)
$\{D_1\}$, $\{D_3\}$, $\{D_4\}$	integral over a single array of in-plane, out-of-plane and twist mode shapes, respectively; Equation (12d), Table 4
e	universal logarithmic constant having an approximate value of 2.71828
e_0	distance from boom centerline to blanket centerline, Figure 4

EI	boom flexural rigidity, Table 2
f_a	force exerted by array tensioning spring, Table 2
f_0	force acting along a single torsion control line, Table 2
F_0	amplitude of nutational forcing function acting on the arrays, Equation (A.7c)
$\{F\}$	forcing function applied to roll/yaw state vector, Equation (14b)
g	gravitational acceleration constant
$[G_{\bar{\alpha}}]$	generalized stiffness for twist modes
GMT	Greenwich Mean Time
$\underline{h}_0$	angular momentum bias vector, Section 2.3 and Figure 1(a)
$[I]$	system mass moment of inertia tensor
I_{px}, I_{py}, I_{pz}	mass moment of inertia of tip pallet about the pallet centre of mass, Figure 1 and Table 2
$\{I_T\}$	matrix made up of integrals of the second moment of twist modes, Equation (12h)
JG	boom torsional rigidity, Table 2
$[J_{\bar{\alpha}}]$	inertia matrix associated with generalized twist coordinates
k_2	effective spring constant between inboard pallet and elevator arm assembly, Figure 4 and Table 2
k_3	effective spring constant between blanket and tip pallet, Figure 4 and Table 2
k_D	damper stiffness

K	parameter which embodies effect of interaction between attitude motion and vibration, Equation (B.3g)
K_I	spacecraft inertia ratio used in Section 2.2.2
$[K_\varepsilon]$	stiffness matrix associated with generalized coordinates ε = U,W; Equations (5b) and (12b)
ℓ_1, ℓ_2	length of boom and blanket respectively; Figure 4
m_D	damper mass
m_1, m_2	mass of tip and inboard pallets, respectively; Figure 4, Table 2
m_s	total mass of satellite
$[M_\varepsilon]$	mass matrix associated with generalized coordinates ε = U,W; Equations (5a) and (12a)
NESA-B	non-spinning Earth sensor
O	spacecraft center of mass when undeformed
O_c	instantaneous spacecraft center of mass (coincides with 'O' when spacecraft undeformed)
O_i	offset of base of ith appendage from 'O'
O_I	force center of orbit, Figure 1
P_ε	frequency for degree of freedom ε = 1, D or N; Appendix A
Q_k	mode shape for kth 'constrained' mode
rpm	revolutions per minute
$[R]$	a coefficient matrix for first order pitch dynamics, Equation (17b)

R_1, R_2, R_3	offset of '0_i' relative to undeformed spacecraft center of mass, measured along roll, pitch and yaw directions, respectively; Figure 1(a) [if '0' coincident with '0_c']
$\{S_1\}, \{S_3\}$ $\{S_5\}, \{S_6\}$	combined in-plane, out-of-plane first moment mode shape effects; Equations (12e), (12f)
t	time
T	system kinetic energy
u_i, v_i, w_i	general vibrational displacement of mass element dm_i along x_i, y_i, z_i directions, respectively; Figure 1(b) and Equations (3)
$\{U_i(t)\}$ $\{W_i(t)\}$	generalized coordinates for in-plane, out-of-plane vibrations of ith array; Equations (3)
x_D	displacement of damper mass from its equilibrium position, Figure 1(c)
x, y, z	body-fixed coordinate system with origin at 0 and aligned with orbiting reference $\underline{1}$, $\underline{2}$, $\underline{3}$ in the equilibrium state
x_i, y_i, z_i	local appendage coordinate system with origin at 0_i, Figure 1(b)
$\{X_k\}, \{Y_k\}$	eigenvectors associated with eigenvalue problem and its adjoint, Equations (15) and (18)
$\{z\}, \{z_1\}$ $\{z_2\}$	state vectors associated with roll/yaw or pitch dynamics, Equations (13) or (16)

$\underline{1},\underline{2},\underline{3}$ orbiting reference frame having its origin at 0_C, with $\underline{1}$ tangent to trajectory, $\underline{2}$ parallel to orbit normal and $\underline{3}$ pointing along local vertical toward 0_I; Figure 1(a)

Greek Symbols

$\alpha_i(y_i, t)$	twist deformation of ith array
$\{\overline{\alpha}_i(t)\}$	generalized coordinates for discretized form of twist coordinate $\alpha_i(t)$, Equation (3c)
β	factor relating constrained, unconstrained damping and frequency; Equations (B.3d), (B.3e), (B.3f)
$\gamma(t)$	array orientation relative to spacecraft central body, Figure 1(a)
δ	logarithmic decrement
$[\Delta_1],[\Delta_3]$	perturbations to generalized mass in-plane, out-of-plane due to shifts in center of mass associated with deformation; Equations (12g)
ε	dummy index used as a general representation for degree(s) of freedom, e.g. ε = U,W
ζ	equivalent linear viscous damping ratio of 'unconstrained' mode
λ_k	kth eigenvalue, Equations (15), (18)
ρ_1,ρ_2	linear mass density for the array boom and blanket, respectively; Table 2
σ	equivalent linear viscous damping ratio of 'constrained' mode

ϕ, θ, ψ Euler rotations defining satellite librational motion of body-fixed x,y,z axes relative to the orbiting reference $\underline{1}$, $\underline{2}$, $\underline{3}$

ϕ_N phase angle given by Equations (A.9b), (A.9c)

$\{\Psi\}, \{\Phi\}, \{\Lambda\}$ sets of assumed mode shapes corresponding to in-plane, out-of-plane and twist deformations; Equations (3)

ω_0 nominal orbital angular velocity of spacecraft center of mass

ω_k 'unconstrained' frequency of kth mode

$\omega_1, \omega_2, \omega_3$ inertial angular velocity of x,y,z coordinate system expressed in terms of components in the $\underline{1}$, $\underline{2}$, $\underline{3}$ reference frame; Equations (1)

Ω_k 'constrained' frequency of kth mode

Subscripts

$(\quad)_D$ damper

$(\quad)_{eq}$ equivalent

$(\quad)_i$ ith appendage

$(\quad)_k$ kth mode

$(\quad)_{k,IP}$, kth mode for the in-plane degrees of freedom

$(\quad)_{k,OOP}$ kth mode for the out-of-plane degrees of freedom

$(\quad)_{k,TWIST}$ kth mode for the twist degrees of freedom

$(\quad)_n$ nth mode

$(\quad)_N$ nutational mode

$(\ )_s, (\ )_a$ symmetric, antisymmetric; Equations (6)

Superscripts

$(\ )',(\ )''$	primes used to distinguish between coordinate systems; Figures 1(b) and 4
$(\ )^*$	refers to a result based on a hysteretic damping law

Miscellaneous

$\frac{\partial(\ )}{\partial(\ )}$	partial derivative operator
$(\dot{\ })$	$\frac{d()}{dt}$
$O()$	of order ( )
$\{\ \}$	column matrix
$[\ ]$	square matrix
$\{\}^T,[\ ]^T$	matrix transpose
$(\underline{\ })$	vector quantity

Symbols are as described here unless otherwise defined for local use (e.g. Appendices). It is common to relax matrix notation using the symbol without an identifying bracket. Aside from 'rpm', MKS units are adopted throughout. Also, all damping factors are negative, but only magnitudes are given in the tables.

1.0 INTRODUCTION

It is generally recognized that improvement is needed in methods for forecasting the damping characteristics of spacecraft structures. The need for improvement stems from the current trend towards spacecraft that are so large and flexible that conventional laboratory measurement of structural properties of the completely-assembled spacecraft is impossible due to gravitational loads.

A method of synthesizing damping that is straightforward in principle is: (i) establish a mathematical model that includes damping for each substructure and main component, by ground test and or analysis; (ii) mathematically assemble the sub-models into an overall structural model of the spacecraft; (iii) derive modal damping factors, modal frequencies and mode shapes from the overall model by eigenproblem analysis. The method is, of course, an extension of standard practice for calculating modal frequencies and mode shapes for situations where damping can be ignored. With damping included in the procedure, a number of practical difficulties are encountered. Tractable models of damping of the subparts are difficult to establish and are often unreliable. This is particularly true for material damping in members, for components with unrestrained fluids, and for connections between structures. Also,differences between gravitational, thermal and vacuum conditions in orbit and on the ground add complication and uncertainty to the process. Inadvertant omission of damping sources is a potential problem as well.

Truncation of modes and off-diagonal damping matrix terms can also contribute errors, the extent being dependent on how the substructure data is handled and how the eigenproblem is solved. There are few documented case studies where damping factors synthesized by this type of method are compared to measured results, and hence the degree to which this type of method is successful, and the limitations, are not yet very well established. References 1-4 and associated cited works are among the recent contributions to damping synthesis.

In Reference 3, a method of the above-described type was applied using ground test data and compared with some of the flight results from the Hermes satellite*. Data on damping that was derived from ground test of a large flexible solar array substructure was first used to calculate damping factors for the satellite in its orbit state; then the calculated damping factors were compared with corresponding values that were measured in-orbit. Calculations were done with both viscous and hysteretic damping laws. In many cases, the in-orbit measured values were higher than the calculated ones by a factor of 2 or 3. While the agreement is representative of current practice, it is not very good. Possible reasons for the differences are: (i) the influence of additional unmodelled damping sources such as fuel motions, a heat pipe, a liquid mercury damper and dissipation in joints connecting the substructures; (ii) the damping models (viscous or

---

*Also known as the Communications Technology Satellite (CTS).

hysteretic) of the array being in error; (iii) inaccuracies introduced into the mathematics as a result of modal truncations and diagonalization of damping coefficient matrices; (iv) a difference in array condition between the ground test and in-orbit state that changes the damping mechanisms (for example altering the state of joint tension, material stress). Due to time and funding limitations, this lack of agreement was not analyzed to any extent at the time (1976). Between 1976 and the end of the mission in 1980, a great deal more flight data was acquired from Hermes. The data confirmed the original measurements reported in Reference 3 and established that the damping values were essentially constant with time. In addition, measurements for several more flexible modes were made[5-7]. Damping information on the nutational mode, with momentum wheel spinning[8] and despun[9], was also obtained.

The purpose of this report is twofold. First, to demonstrate a synthesis procedure for spacecraft damping factors that uses a rigorous eigenvalue analysis involving damped modes (as opposed to procedures that use undamped modes), via application to the Hermes satellite configuration (a gyroscopic system with distributed and discrete dampers). Second, to use this synthesis method in conjunction with the Hermes substructure level and spacecraft level flight data, with a view to determining how well the method performs and to improving the understanding of the damping mechanisms of Hermes.

More specifically, in Chapter 2 a model for a satellite structure consisting of central rigid body, 2 flexible solar arrays, a momentum wheel and a liquid mercury damper is first developed in the form corresponding to Reference 10 and 11. The mathematical formulation used is described in Reference 10, and is similar in principle to that of References 2 and 3, but it eliminates uncertainties associated with diagonalization of damping matrices. Modal analysis for an array as a fixed-base-mounted substructure is also given in Chapter 2. In the third chapter, flight-derived measurements of Hermes are updated and summarized. Calculations with various parameter sets are then presented, with a view to investigating the role of the liquid mercury damper, the sources of damping of the nutational mode, and the extent to which damping factors of the solar array substructure can be related to damping factors of the overall satellite. In Appendix A, functional relationships between component damping factors and the damping factor of the nutational mode are derived using the Method of Averaging and are used to confirm software and predictions associated with the eigenvalue analysis.

2.0 MODEL FOR SPACECRAFT MODAL INFORMATION BASED ON SUB-MODELS OF SYSTEM SUBSTRUCTURES AND COMPONENTS

In this chapter, the mathematical model of the substructures, components, and overall spacecraft of the Hermes type is outlined. Reference 11 gives a detailed derivation in the discretized form (before transformation to modal variables) for the model of the spacecraft, minus the liquid mercury damper. The reader is referred to References 10 and 11 for supplementary explanation of the methods and details.

2.1 Spacecraft Configuration and Kinematics

The satellite consists of a central rigid body, two flexible solar arrays, a liquid mercury damper and a momentum wheel, configured as shown in Figure 1. The reference frame (Oxyz) is attached to the central rigid body, with O at the nominal system mass center (without deformation) of the total configuration. The arrays rotate about the Oy axis together and nominally track the sun. The central body nominally tracks the earth. The angle between the arrays and the central body is denoted by γ, and its rate is maintained constant at one revolution per day by a drive and track mechanism. (O_c, $\underline{1}$, $\underline{2}$, $\underline{3}$) is an orthogonal orbiting reference frame with origin fixed at the instantaneous mass center O_c, $\underline{1}$ aligned along the tangent to the trajectory in the direction of motion, $\underline{2}$ parallel to the orbit normal and $\underline{3}$ pointing inward along

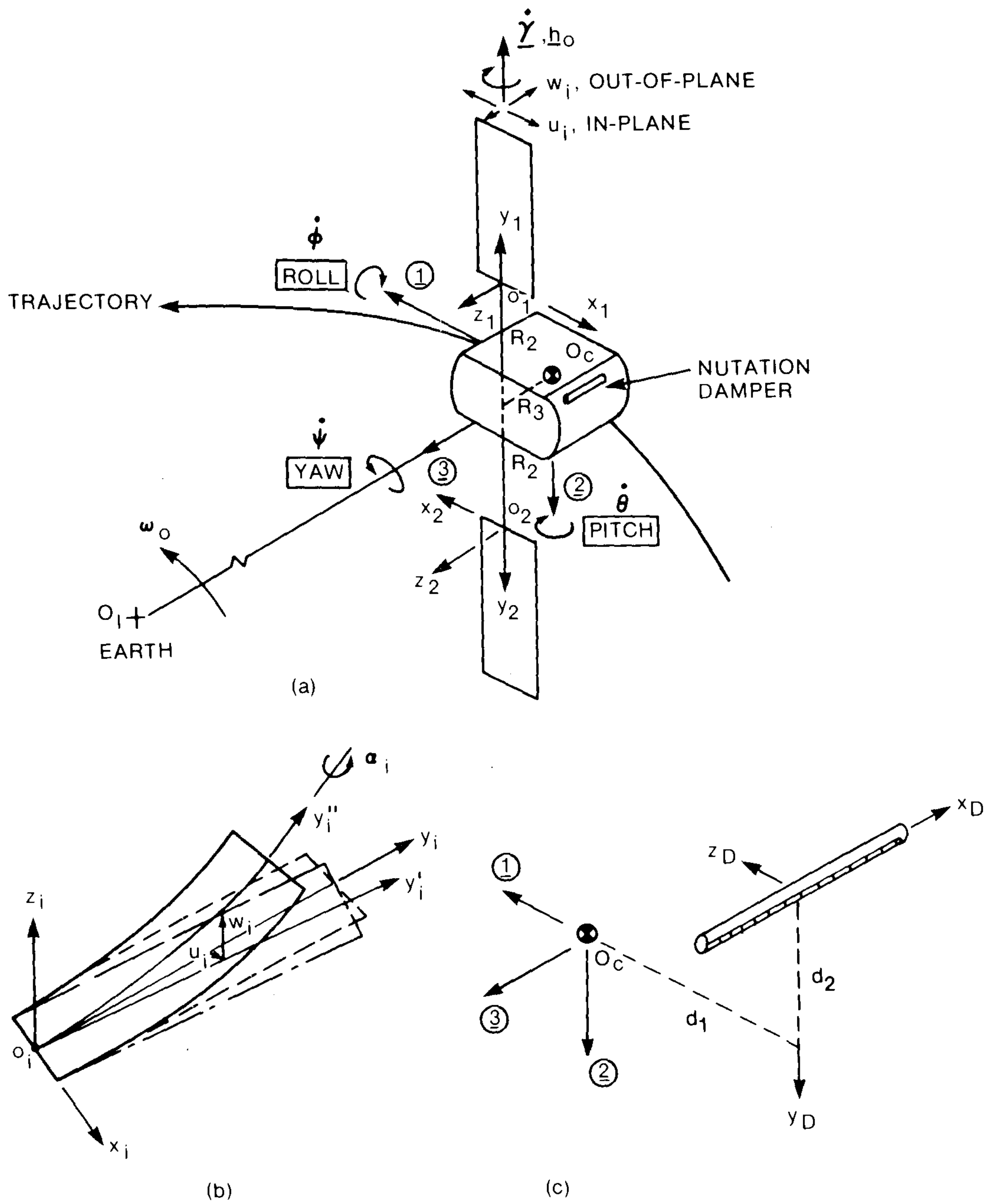

FIGURE 1 Schematic for the Hermes class of spacecraft: (a) overall configuration; (b) array coordinates detailing in-plane (u_i), out-of-plane (w_i) and twist (α_i); (c) offset and coordinates of nutation damper.

the local vertical towards the center of the earth. The frame is thus rotating about the Oz axis at the negative of the orbit rate ($-\omega_0$).

Satellite attitude motion is defined by Eulerian rotations ϕ (roll), θ (pitch), ψ (yaw) of body-fixed frame $(0, x, y, z)$ with respect to the orbit frame (0_c, $\underline{1}$, $\underline{2}$, $\underline{3}$).

The central body rotates relative to inertial space with rates $(\omega_1, \omega_2, \omega_3)$, which in turn are related to pitch, roll and yaw rates, to linear order, by

$$\omega_1 = \dot{\phi} - \omega_0 \dot{\psi}; \tag{1a}$$

$$\omega_2 = \dot{\theta} - \omega_0; \tag{1b}$$

$$\omega_3 = \dot{\psi} + \omega_0 \dot{\phi}. \tag{1c}$$

2.2 Nutation Damping

2.2.1 The Liquid Mercury Damper

The nutation damper considered herein is a cylindrically-shaped tube partially filled with mercury and aligned parallel to the pre-deployment spin axis, as is depicted schematically in Figure 1. The modelling is not straightforward and further, it is difficult to verify by ground test because of Earth gravity effects. Both geometric parameters (size, orientation and offset with respect to center of mass) and dynamic parameters (mass, natural frequency, energy dissipation rate, spin rate, gravitational field) play a role in determining the damper's performance. Several techniques have been suggested to obtain simple models that are amenable for use in satellite simulations. Reference 12 treats the fluid as a rigid slug of finite dimension. Reference 13 provides a classic inviscid potential flow representation governed by the Laplace equation. References 14 and 15 allude to linear analytic solutions for laminar flow, expressible as a complex series of Bessel functions. A simplified approach adopted in Reference 14 involves a Poiseuille flow. Results exist as well for turbulent flow.[14-16] Another simplification that is often used successfully is to employ 'energy-sink' analysis wherein it is assumed that the moments exerted by the damper on the spacecraft are negligible but not vice versa.[17] Analytic predictions alone, however, often do not reliably establish damper performance.[17]

2.2.2 The Hermes Spin Phase

The Hermes liquid mercury damper was designed for the specific purpose of damping out the nutation associated with the spin phase, before deployment of the arrays and spin-up of the momentum wheel. Principles governing operation of this type of damper are discussed in general terms in References 18 through 20, but unfortunately the exact models used are not fully presented. Reference is made to internal Hughes documents, none of which are available in the open literature. Based on available literature, the following picture of the damping process emerges.

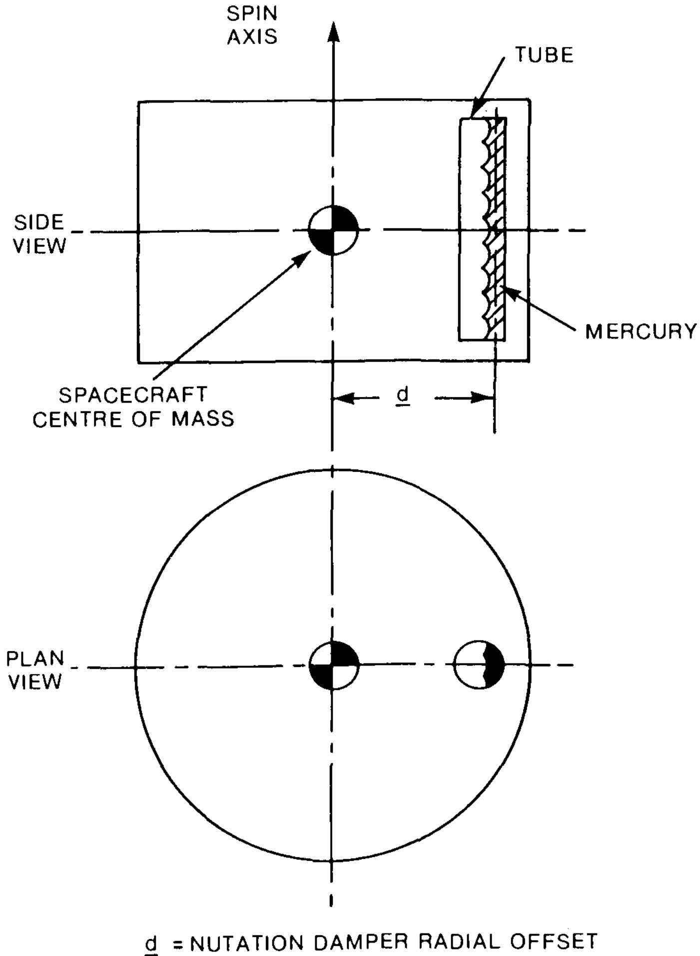

FIGURE 2 Partially-filled liquid mercury damper offset relative to overall spacecraft centre of mass.

Centrifugal forces due to spin cause the fluid to distribute along one side of the tube (Figure 2). The damper is considered 'tuned' in the sense that natural frequency associated with standing surface waves is made to equal the nominal nutational frequency by appropriate choice of tube length. This produces a maximum damping effect for small nutations. Energy is dissipated through fluid viscosity. The mechanism is somewhat different at large nutation angles, where both momentum transfer and friction are involved as the fluid becomes a series of separate packets continuously colliding, breaking up, and reforming again. Design parameters are listed in Table 1.

Table 1

Design Parameters for the Hermes Liquid Mercury Nutation Damper

Mercury Density	1.3545×10^{4} kg. m^{-3}		
Mercury Viscosity	0.016	poise	
Cavity Fill Fraction	20%		
Internal Tube Diameter	1.23×10^{-2}	m	(0.485")
Cavity Length	0.356	m	(14.0")
Mass of Mercury in Tube	0.114	kg	(0.25 lb)
Mass of Tube + Mercury	0.386	kg	(0.85 lb)
Radial Offset from Centre of Mass, d	0.838	m	(33")

The damper design, of the type used for Hermes was apparently tested at Hughes by suspension as a pendulum horizontally mounted with bifilar supports.[18-21] The difficulties encountered are: it is necessary to scale in differences between a one-g test environment and the in-orbit centrifugally generated field of ≃ 3 g (spin-stabilized phase); plus surface tension precludes maintenance of an invariant Reynolds number. The net design predictions, based on preflight theory and experiment, are given in Figure 3. Displayed is the time constant corresponding to a decrease in amplitude by a factor of 1/e as a function of spacecraft inertia ratio, $K_I^* = I_{spin}/I_{transverse}$. The damper is tuned so that maximum damping occurs at $K_I = 1.35$ corresponding to a nominal nutation rate of about 0.40 Hz at 60 rpm spin. Little variation occurs in level of performance at spin rates between 54 rpm and 66 rpm over inertia ratios ranging from 1.2 to 1.5.[19]

---

*for triaxial satellite $K_I = Izz/\sqrt{Ixx\ Iyy}$

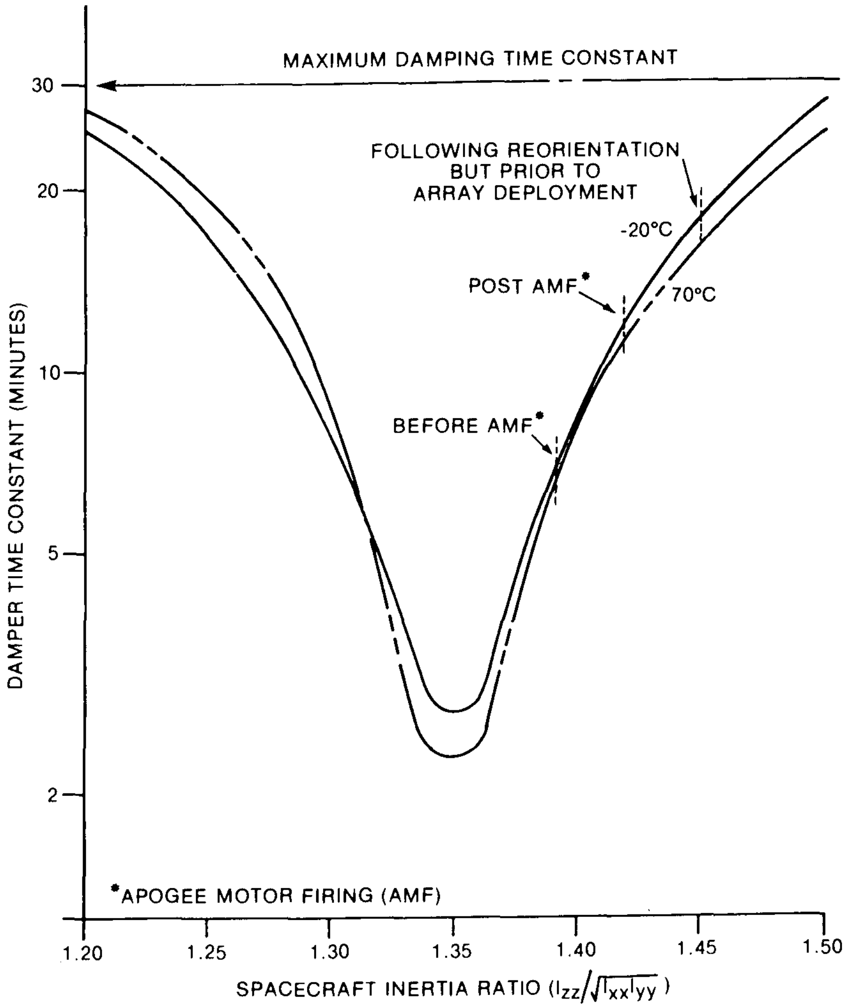

FIGURE 3 Design information on the Hermes damper as calculated before launch. Optimum performance is achieved at a 20% fill fraction for a 54 rpm spin rate.

Following separation of the satellite from the launch vehicle, K = 1.39, the spin-rate was 1.03 Hz, the nutation rate was 0.41 Hz and a 0.5° nutation damped out in 120 seconds; this data yielded a damping ratio of 0.007.[22] Immediately following apogee motor burn, K = 1.42, the spin rate was 1.00 Hz, the nutation rate was 0.44 Hz, and a 0.4° nutation damped out in 350 seconds; this data yielded a damping ratio of 0.001. These two operating states are noted in Figure 3 where it is seen that significantly larger damping times are predicted. Thus one concludes that the forecast performance of Figure 3 and associated pre-launch calculations are based on a conservative model.

2.2.3 The Hermes 3-Axis Stabilized Configuration

While not originally designed to provide damping for the spacecraft in the 3-axis stabilized phase with arrays fully deployed, the damper is not caged and therefore it still has an effect. The damper is excited by roll/yaw nutation, pitch axis librations, and by symmetric and antisymmetric array vibrations (note the geometry in Figure 2). The nominal tuned frequency of the damper, at 0.40 Hz, is close to the frequency of an in-orbit mode(the fundamental out-of-plane antisymmetric vibration at about 0.44Hz[5-7]) and therefore the potential for resonance exists.

For this phase, the spacecraft motion consists of a combination of a slow rotation about pitch (once in 24 hours), a small low frequency nutation (0.2° at 2.77×10^{-3} Hz), and flexing of the various structural modes (at 0.15 Hz and higher). Relation of the damper's operation in this dynamical environment to earth-based test or spin phase operation is not possible. The fluid might be spread out uniformly in the tube as in Figure 2 due to the centrifugal force of the slow rotation. Alternately, it is possible that surface tension effects cause the mercury to form a single or several slugs.

Due to the uncertainties and complexities associated with the fluid behaviour, the sole reasonable approach for Hermes (and the one adopted herein) is to model the damper as a single degree of freedom translational mass-spring-dashpot device located as in Figure 1. The mass (m_D) is the actual mass of the mercury and is assumed to be a slug in equilibrium at $(-d_1, -d_2)$ in $(Oxyz)$, and the dashpot and spring parameters (c_d and k_D) are selectable to match desired damper energy dissipation and resonance characteristics. Although the c_D and k_D cannot be obtained with certainty for Hermes, by varying these parameters the range of possible influence of the damper on the spacecraft can be established. This approach was used in modelling a similar damper on SYNCOM[17] where the effective spring was due to centrifugal force. In fact, such a representation is common in the literature.[23-25] With the nutation damper fixed in space, the kinetic, potential and dissipation functions are, respectively:

$$\tfrac{1}{2}m_D\dot{x}_D^2 \quad ; \quad \tfrac{1}{2}k_D x_D^2 \quad ; \quad \tfrac{1}{2}c_D\dot{x}_D^2 \quad . \tag{2a}$$

The stiffness and damping constant can be further expressed in terms of damper frequency and damping ratio by:

$$k_D = m_D\Omega_D^2 \quad ; \quad c_D = 2m_D\Omega_D\sigma_D \quad . \tag{2b}$$

2.3 Momentum Wheel

The momentum wheel is assumed to spin at constant speed, relative to the central body, and to be aligned so that its angular momentum vector $\underline{h}_0$ points in the negative Oy direction.

2.4 Solar Arrays

Each solar array substructure is described in the overall system model by specifying its fixed-base (constrained) modal data, namely modal frequencies (Ω's), mode shapes (Q's) and modal damping factors (σ's). The substructure model adopted here is described in section 2.4.1.

As is the usual case for such substructures, the modal data is obtained from a combination of analysis and test. Because damping is small for the solar arrays, the determination of modal frequencies and shapes (Ω's and Q's) can be discussed separately from determination of damping factors (σ's). The former are discussed in 2.4.2, and the latter in 2.4.3.

2.4.1 Substructure Model

Each array consists of a boom, a blanket, pallets, and ancillary equipment as depicted in Figure 4. A coordinate system (O_i, x_i, y_i, z_i) is attached to each array which itself is attached to the central body as depicted in Figure 1, in such a manner that there are offset distances R_2 and R_3 between the attachment point

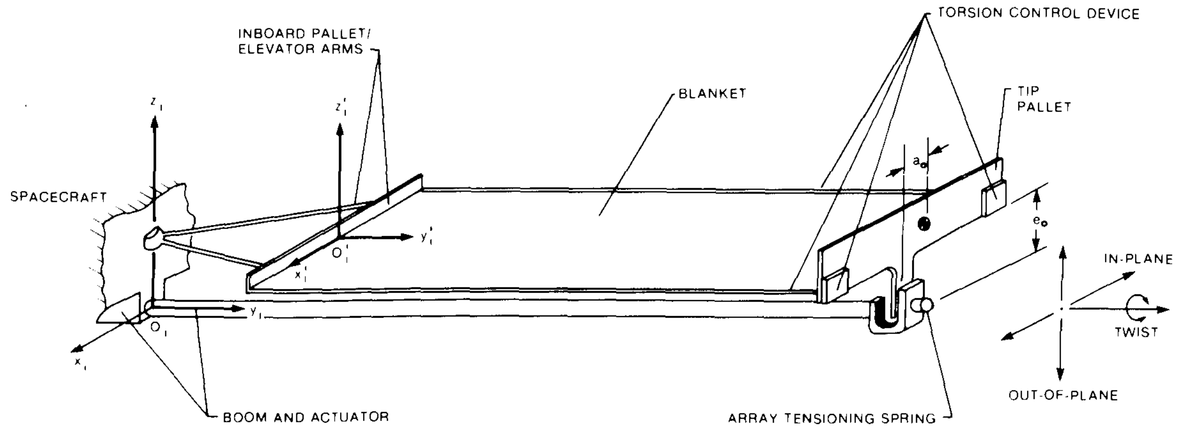

FIGURE 4 Essential elements of the Hermes solar array model.

and the center of mass of the overall spacecraft configuration. The deformation at a field point in an array can be visualized as being the sum of an out-of-plane (w_i), an in-plane (u_i) and a twist (α_i) component. The deformations are discretized in the spirit of the Rayleigh-Ritz method as follows for the north (1) array:

$$u_1(x_1, y_1, z_1, t) = \Psi^T(y_1)\ U_1(t); \tag{3a}$$

$$w_1(x_1, y_1, z_1, t) = \Phi^T(y_1)\ W_1(t); \tag{3b}$$

$$\alpha_1(x_1, y_1, z_1, t) = \Lambda^T(y_1)\ \bar{\alpha}_1(t). \tag{3c}$$

$U_1(t)$, $W_1(t)$ and $\overline{\alpha}_1(t)$ are column matrices of time dependent coordinate variables. Similarly coordinates $U_2(t)$, $W_2(t)$, and $\overline{\alpha}_2(t)$ can be defined for the south (2) array. Ψ, Φ, and Λ are column matrices of shape factors and are chosen identical for each array. The solar array parameters can be defined in terms of stiffness, mass, and damping matrices corresponding to their coordinates. If the base of the array is fixed, the kinetic, potential and dissipation functions are, repectively, for the north array:

$$\tfrac{1}{2}\dot{U}_1^T \; M_U \dot{U}_1 \; + \; \tfrac{1}{2}\dot{W}_1^T M_W \dot{W}_1 \; + \; \tfrac{1}{2}\dot{\overline{\alpha}}_1^T J_{\overline{\alpha}} \; \dot{\overline{\alpha}}_1 \qquad ; \tag{4a}$$

$$\tfrac{1}{2}U_1^T \; K_U U_1 \; + \; \tfrac{1}{2}W_1^T K_W W_1 \; + \; \tfrac{1}{2}\overline{\alpha}_1^T G_{\overline{\alpha}} \; \overline{\alpha}_1 \qquad ; \tag{4b}$$

$$\tfrac{1}{2}\dot{U}_1^T \; C_U \dot{U}_1 \; + \; \tfrac{1}{2}\dot{W}_1^T C_W \dot{W}_1 \; + \; \tfrac{1}{2}\dot{\overline{\alpha}}_1^T C_{\overline{\alpha}} \dot{\overline{\alpha}}_1 \qquad . \tag{4c}$$

In the overall spacecraft model, each array is described in terms of fixed-base (constrained) modal data, namely, modal frequencies, shapes and damping factors. The Ψ, Φ, and Λ are such that the out-of-plane, in-plane, and twist motions are uncoupled, consequently the array dynamics is simplified and M, K, C matrices are then diagonal, and related to the basis modal data by:

$$M_{U\,k} = \int (Q_U)_k^T \, (Q_U)_k \, dm; \quad M_{W\,k} = \int (Q_W)_k^T \, (Q_W)_k \, dm;$$

$$J_{\bar{\alpha}\,k} = \int (Q_{\bar{\alpha}})_k^T \, (Q_{\bar{\alpha}})_k \, dm; \tag{5a}$$

$$K_U = M_U \Omega_U^2 \; ; \quad K_W = M_W \Omega_W^2 \; ; \quad G_{\bar{\alpha}} = J_{\bar{\alpha}} \Omega_{\bar{\alpha}}^2 \; ; \tag{5b}$$

$$C_U = 2 M_U \Omega_U \sigma_U ; \; C_W = 2 M_W \Omega_W \sigma_W \; ; \; C_{\bar{\alpha}} = 2 J_{\bar{\alpha}} \Omega_{\bar{\alpha}} \sigma_{\bar{\alpha}} \, . \tag{5c}$$

This representation presupposes that damping of the solar array can be modelled by equivalent linear viscous modal damping terms. The effect of presupposing a hysteretic damping model of the type described in References 3 and 26 is also assessed qualitatively by scaling damping factors according to the appropriate frequency ratios, in connection with analysis of some of the Hermes flight data (Chapter 3).

Because the arrays and overall configuration are symmetric, it is convenient to transform the pairs of coordinate variables for north and south arrays to 'symmetric' and 'antisymmetric' coordinate variables, by:

$$U_s = \tfrac{1}{2}(U_1 - U_2); \quad U_a = \tfrac{1}{2}(U_1 + U_2) \; ; \tag{6a}$$

$$W_s = \tfrac{1}{2}(W_1 + W_2); \quad W_a = \tfrac{1}{2}(W_1 - W_2); \tag{6b}$$

$$\bar{\alpha}_s = \tfrac{1}{2}(\bar{\alpha}_1 - \bar{\alpha}_2); \quad \bar{\alpha}_a = \tfrac{1}{2}(\bar{\alpha}_1 + \bar{\alpha}_2). \tag{6c}$$

2.4.2 Constrained Modal Frequencies and Shapes

The constrained modal frequencies and mode shapes were obtained before launch for Hermes as follows. An analytical structural model was derived for the array in the fixed-base configuration in ground test (i.e. with gravitational forces included), in terms of physical coordinates and analytical stiffness and mass matrices. From the model, mode shapes and modal frequencies for the one-g state were obtained by solving the undamped eigenvalue problem. Experimentally measured modal frequencies and modal damping factors were also determined in ground tests. Then the analytical model and ground test results were brought into agreement by appropriate adjustments to the analytical model.[6] In turn, this model was then used to calculate in-orbit modal frequencies and shapes by setting g equal to zero. Results derived in this manner are documented in References 27-29.

For the present report, the model and computer program of References 27, 28 were used. Geometric offset parameters a_0 and e_0 were set equal to zero, so that the modes uncoupled into three sets: namely, out-of-plane, in-plane and twist. As well, the computer program was extended to calculate the modal coefficients and integrals needed in Chapter 2.5. Tables 2 and 3 give the parameters and data as used in the calculations.

TABLE 2

Parameter Summary for a Single Solar Array of Hermes

PARAMETER	VALUE	UNITS
a_0	0	m
e_0	0	m
ℓ_1	7.23	m
ℓ_2	6.50	m
b	1.311	m
b^1	0.655	m
ρ_1	0.2925	$kg.m^{-1}$
ρ_2	1.060	$kg.m^{-1}$
m_1	4.42	kg
m_2	3.40	kg
I_{px}	0.556	$kg.m^2$
I_{py}	0.026	$kg.m^2$
I_{pz}	0.556	$kg.m^2$
k_2	1220.	$N.m\ RAD^{-1}$
k_3	1356.	$N.m\ RAD^{-1}$
f_a	35.59	N
f_o	1.33	N
EI	868.	$N.m^2$
JG	1.07	$N.m^2.RAD^{-1}$
g	9.81	$m.s^{-2}$

TABLE 3

Modal Frequencies and Related Integral Coefficients of the Fixed Base (Constrained) Hermes Array

QUANTITY	MODE NUMBER, k 1	2	3	4	5
Out-of-plane					
$(M_W)_{kk}$, kg	2.3353	6.171×10^{-2}	3.228×10^{-3}	1.625×10^{-3}	1.587×10^{-4}
$(K_W)_{kk}$, $N.m^{-1}$	2.0349	6.229×10^{-1}	1.167×10^{-1}	3.975×10^{-1}	8.429×10^{-1}
$D_{3_k}=\int\Phi_k dm$, kg	4.9955	2.349×10^{-1}	3.625×10^{-2}	2.747×10^{-2}	6.947×10^{-3}
$B_{3_k}=\int y_k\Phi_k dm$, kg.m	30.463	6.419×10^{-2}	3.823×10^{-2}	4.192×10^{-2}	2.363×10^{-2}
Ω_k, Hz	0.1486	0.5056	0.9570	2.489	11.60
In-Plane					
$(M_U)_{kk}$, kg	1.9124	7.852×10^{-4}	1.517×10^{-4}		
$(K_U)_{kk}$, $N.m^{-1}$	7.9256	3.310×10^{-1}	2.2237		
$D_{1k} = \int\Psi_k dm$, kg	4.5468	1.822×10^{-2}	3.996×10^{-3}		
$B_{1k} = \int y_k\Psi_k dm$, kg.m	27.439	3.009×10^{-2}	3.177×10^{-3}		
Ω_k, Hz	0.3240	3.268	19.27		
Twist					
$(J_{\bar{\alpha}})_{kk}$, $kg.m^2$	0.6371	7.817×10^{-3}	3.233×10^{-4}		
$(G_{\bar{\alpha}})_{kk}$, N.m/RAD	0.5192	7.502×10^{-2}	1.092×10^{-2}		
$D_{4_k} = \int\Lambda_k dm$, kg	9.8383	3.543×10^{-1}	4.255×10^{-2}		
$I_{Tk} = \int x_k^2\Lambda_k dm$, $kg.m^2$	1.373	-6.149×10^{-3}	7.051×10^{-3}		
Ω_k, Hz	0.1437	0.4931	0.9247		

By comparing the relative values (e.g. M_{11}, M_{22} etc.) for the mass-related coefficients (M's, B's and D's), it is seen that the fundamental mode of each category is dominant, thus ensuring that truncation to the first few modes is valid.[30]

2.4.3 Constrained Modal Damping Factors From Ground Test

Unlike modal frequencies and shapes, substructural modal damping factors cannot be obtained with confidence from analysis

TABLE 4

Modal Damping Factors For The Fixed-Base (Constrained) HERMES Array As Determined Using Ground Test And Adjusted By Analysis to g = 0 (Reference 3)

MODE	FREQUENCY	DAMPING RATIO
Out-of-plane		
1	0.16	0.003* - 0.006**
2	0.51	0.008 - 0.012+
In-plane		
1	0.32	0.014 - 0.020
Twist		
1	0.15	0.090 - 0.160
2	0.50	0.013 - 0.022

* based on 'hysteretic' damping law
** based on 'viscous' damping law
\+ constructed using Table 1 of Reference 3

only. They cannot be measured directly in ground tests either, because of the earth's gravitation effect on the structure.

Table 4 presents array damping factors that were obtained in Reference 3 from a combination of one-g test data and one-g to zero-g conversion analysis. Although the values are not promoted as being completely trustworthy, they were the only ones available for this type of solar array (further conclusions regarding their validity are obtained later in this report).

2.5 Spacecraft Model in Terms of Discrete Coordinate Variables

With the preceding definition of variables and parameters, governing equations for the mathematical model of the overall satellite configuration can be derived using the methods of References 10 and 11. Resulting equations follow.

$$I_{11}\dot{\omega}_1 + I_{13}\dot{\omega}_3 + h_0\omega_3 - 2\sin\gamma S_1^T\ddot{U}_a - 2\cos\gamma S_3^T\ddot{W}_a - m_D d_2\ddot{x}_D$$

$$= L_1 \quad ; \tag{7a}$$

$$I_{33}\dot{\omega}_3 + I_{13}\dot{\omega}_1 - h_0\omega_1 - 2\cos\gamma S_1^T\ddot{U}_a + 2\sin\gamma S_3^T\ddot{W}_a = L_3 \quad ; \tag{7b}$$

$$I_{22}\dot{\omega}_2 + 2S_5^T\ddot{U}_s - 2S_6^T\ddot{W}_s - 2I_T\ddot{\bar{\alpha}}_s + m_D d_1 (\ddot{x}_D - d_2\dot{\omega}_1) = L_2 \,. \tag{7c}$$

$$M_U\ddot{U}_a + C_U\dot{U}_a + K_U U_a - (\sin\gamma\dot{\omega}_1 + \cos\gamma\dot{\omega}_3)S_1 = 0 \quad ; \tag{8a}$$

$$M_W\ddot{W}_a + C_W W_a + K_W W_a - (\cos\gamma\dot{\omega}_1 - \sin\gamma\dot{\omega}_3)S_3 = 0 \quad . \tag{8b}$$

$$(M_U - \Delta_1)\ddot{U}_S + C_U\dot{U}_s + K_U U_s + S_5\dot{\omega}_2 = 0 \quad ; \tag{9a}$$

$$(M_W - \Delta_3)\ddot{W}_s + C_W\dot{W}_s + K_W W_s - S_6\dot{\omega}_2 = 0 \quad . \tag{9b}$$

$$J_{\bar{\alpha}}\ddot{\bar{\alpha}}_s + C_{\bar{\alpha}}\dot{\bar{\alpha}}_s + G_{\bar{\alpha}}\bar{\alpha}_s - I_T\dot{\omega}_2 = 0 \quad . \tag{10}$$

$$m_D\ddot{x}_D + c_D\dot{x}_D + k_D x_D + m_D (d_1\dot{\omega}_2 - d_2\dot{\omega}_1) = 0. \tag{11}$$

In the above equations, coefficients are given by:

$$M_U = \int \Psi\Psi^T dm; \quad M_W = \int \Phi\Phi^T dm; \quad J_{\bar{\alpha}} = \int \Lambda\Lambda^T dm; \tag{12a}$$

$$K_U = \Omega_U^2 M_U; \quad K_W = \Omega_W^2 M_W; \quad G_{\bar{\alpha}} = \Omega_\alpha^2 J_{\bar{\alpha}}; \tag{12b}$$

$$B_1 = \int y\Psi dm; \quad B_3 = \int y\Phi dm; \tag{12c}$$

$$D_1 = \int \Psi dm; \quad D_3 = \int \Phi dm; \tag{12d}$$

$$S_1 = B_1 + R_2 D_1; \quad S_3 = B_3 + R_2 D_3; \tag{12e}$$

$$S_5 = -\cos\gamma R_3 D_1; \quad S_6 = -\sin\gamma R_3 D_3; \tag{12f}$$

$$\Delta_1 = D_1 D_1^T / m_s; \quad \Delta_3 = D_3 D_3^T / m_s; \tag{12g}$$

$$I_T = \int x^2 \Lambda dm. \tag{12h}$$

A complete definition of symbols is given in the Nomenclature. Also, the equations are linearized about the following equilibrium state: $\omega_1 = 0$; $\omega_2 = \omega_0$; $\omega_3 = 0$; $\gamma = \omega_0 t$. Additional simplifications are adopted as outlined on pages 5, 6, and 15 of Reference 11.

Equation (7) is essentially Euler's equation for the total spacecraft, extended to include flexible effects. The three equations express the principle that 'rate of change of angular momentum equals torque' about the roll (L_1), pitch (L_2) and yaw (L_3) axes, respectively.

Equations (8a) and (8b) are the second order vibrational equations which define the time history of the antisymmetric in-plane and antisymmetric out-of-plane deformations, respectively. Equations (9a) and (9b) similarly define the symmetric in-plane and out-of-plane deformations. Equation (10) defines the symmetric twist deformations.

Equation (11) is the second-order equation which defines the time history of the damper oscillation. Equations (7) through (11) constitute complete system equations of motion. In absence of a nutational damper, symmetries inherent in the configuration serve to uncouple dynamics of pitch from roll/yaw. As well, it is seen that symmetric array oscillations interact with pitch only and vice versa. A similar relationship exists between roll/yaw degrees of freedom and antisymmetric bending vibrations. When offset from vehicle center of mass, the damper is coupled directly with pitch and roll but not yaw or array displacements.

2.6 Transformation To The Damped Natural Modes Formulation

Equations (7-11) are converted to modal variables following the formulation outlined in Reference 10. In this method, the equations are transformed to a first order set through introduction of a state vector made up of generalized displacement and generalized velocity. The system matrices are rendered either symmetric, or skew symmetric, by choosing a suitable constraint between generalized velocity and displacement. Algebraic manipulation is used to avoid use of complex numbers when generating response from the resulting eigenvalue problem and its adjoint. Once system eigenvalues and eigenvectors are known, response depends on the solution of coupled, real-valued, scalar, first order equations.

With nutation damping included, roll/yaw and pitch are, in general, coupled. If d_1 is nonzero and d_2 is zero, the damper couples to pitch but not roll/yaw; if d_1, is zero and d_2 is nonzero, the damper couples to roll/yaw, but not to pitch. To reduce confusion and to aid in isolating the effect of the damper, this study is confined to these two bounding cases.

2.6.1 Roll/Yaw and Antisymmetric Deformation Including the Damper

The state vector describing the motion is:

$$\{z\} = \{\omega_1 \quad \omega_3 \quad \dot{U}_a^T \; \dot{W}_a^T \quad \dot{x}_n \quad U_a^T \; W_a^T \; x_n\}^T \quad . \tag{13}$$

Using the methods of Chapter 2 of Reference 10, Equations (7a), (7b), (8a), (8b), and (11) (with $d_1 = 0$) can be written in the following first order form

$$[A]\,\{\dot{z}\} + [B]\{z\} = \{F\} \; ; \tag{14a}$$

where:

$$\{F\} = \{L_1 \quad L_3 \quad 0\;0\;0\;0\;0\;0\}^T \quad ; \tag{14b}$$

$$[A]=\begin{bmatrix} I_{11} & I_{13} & -2s\gamma S_1^T & -2c\gamma S_3^T & -m_D d_2 & 0 & 0 & 0 \\ I_{13} & I_{33} & -2c\gamma S_1^T & 2s\gamma S_3^T & 0 & 0 & 0 & 0 \\ -2s\gamma S_1 & -2c\gamma S_1 & 2M_U & 0 & 0 & 0 & 0 & 0 \\ -2c\gamma S_3 & 2s\gamma S_3 & 0 & 2M_W & 0 & 0 & 0 & 0 \\ -m_D d_2 & 0 & 0 & 0 & m_D & 0 & 0 & 0 \\ 0 & 0 & 0 & 0 & 0 & 2K_U & 0 & 0 \\ 0 & 0 & 0 & 0 & 0 & 0 & 2K_W & 0 \\ 0 & 0 & 0 & 0 & 0 & 0 & 0 & k_D \end{bmatrix}; \quad (14c)$$

$$[B]=\begin{bmatrix} 0 & h_0 & 0 & 0 & 0 & 0 & 0 & 0 \\ -h_0 & 0 & 0 & 0 & 0 & 0 & 0 & 0 \\ 0 & 0 & 2C_U & 0 & 0 & 2K_U & 0 & 0 \\ 0 & 0 & 0 & 2C_W & 0 & 0 & 2K_W & 0 \\ 0 & 0 & 0 & 0 & c_D & 0 & 0 & k_D \\ 0 & 0 & -2K_U & 0 & 0 & 0 & 0 & 0 \\ 0 & 0 & 0 & -2K_W & 0 & 0 & 0 & 0 \\ 0 & 0 & 0 & 0 & -k_D & 0 & 0 & 0 \end{bmatrix} \cdot (14d)$$

Equations (13,14) are in the format of Equations (39), Chapter 3, of Reference 10. The associated eigenvalue problem and its adjoint, which lead to the natural frequencies and damped modes, are:

$$(\lambda_k[A] + [B])\,\{X_k\} = \{0\} \quad ; \tag{15a}$$

$$(\lambda_k[A] + [B]^T)\,\{Y_k\} = \{0\} \ . \tag{15b}$$

Software was developed to solve the eigenvalue problem based on the above equations, and to calculate the natural modes, frequencies, and damping factors. Figure 5 depicts the input, output and flow of calculations.

2.6.2 Pitch and Symmetric Deformation Including the Damper

Similarly, for pitch, one can adopt state vector:

$$\{z\}^T = [z_1^T, \; z_2^T] \quad ; \tag{16a}$$

where

$$\{z_1\}^T = \{\dot{x}_D \quad \dot{U}^T{}_s \quad \dot{W}^T{}_s \quad \dot{\alpha}_s^T\}^T \quad ; \tag{16b}$$

$$\{z_2\}^T = \{x_D \quad U^T{}_s \quad W^T{}_s \quad \bar{\alpha}_s^T\}^T \quad . \tag{16c}$$

Then Equations (7c), (9a), (9b), (10) and (11) (with $d_2 = 0$) can be arranged into the form:

$$I_{22}\,\dot{\omega}_2 + \{C\}^T\{\dot{z}\} = L_2 \quad ; \tag{17a}$$

$$[R]\,\{\dot{z}\} + \{B\}\,\{z\} + \dot{\omega}_2\,\{C\} = \{0\} \quad ; \tag{17b}$$

where,

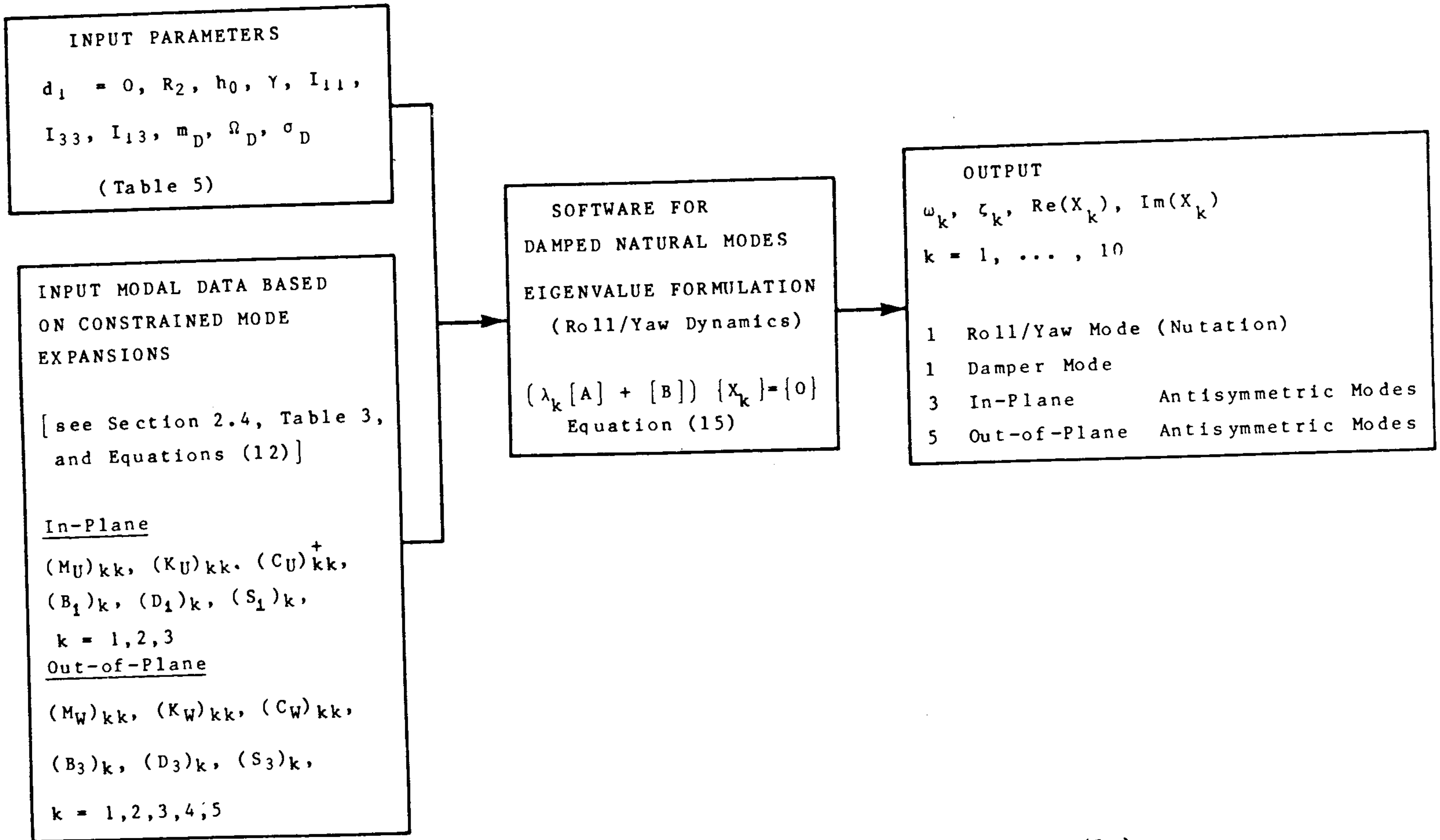

+Note, modal damping coefficients are related to damping ratios by Equations (5c)

FIGURE 5 Damped Natural Modes solution for roll,yaw dynamics.

$$[R] = \begin{bmatrix} m_d & 0 & 0 & 0 & 0 & 0 & 0 & 0 \\ 0 & (M_U-\Delta_1) & 0 & 0 & 0 & 0 & 0 & 0 \\ 0 & 0 & (M_W-\Delta_3) & 0 & 0 & 0 & 0 & 0 \\ 0 & 0 & 0 & J_{\bar{\alpha}} & 0 & 0 & 0 & 0 \\ 0 & 0 & 0 & 0 & k_D & 0 & 0 & 0 \\ 0 & 0 & 0 & 0 & 0 & K_U & 0 & 0 \\ 0 & 0 & 0 & 0 & 0 & 0 & K_W & 0 \\ 0 & 0 & 0 & 0 & 0 & 0 & 0 & G_{\bar{\alpha}} \end{bmatrix} ; \qquad (17c)$$

$$[B] = \begin{bmatrix} c_D & 0 & 0 & 0 & k_D & 0 & 0 & 0 \\ 0 & C_U & 0 & 0 & 0 & K_U & 0 & 0 \\ 0 & 0 & C_W & 0 & 0 & 0 & K_W & 0 \\ 0 & 0 & 0 & C_{\bar{\alpha}} & 0 & 0 & 0 & G_{\bar{\alpha}} \\ -k_D & 0 & 0 & 0 & 0 & 0 & 0 & 0 \\ 0 & -K_U & 0 & 0 & 0 & 0 & 0 & 0 \\ 0 & 0 & -K_W & 0 & 0 & 0 & 0 & 0 \\ 0 & 0 & 0 & -G_{\bar{\alpha}} & 0 & 0 & 0 & 0 \end{bmatrix} ; \qquad (17d)$$

$$\{C\} = \begin{Bmatrix} m_D d_1 \\ 2S_5 \\ -2S_6 \\ -2I_T \\ 0 \\ 0 \\ 0 \\ 0 \end{Bmatrix} . \qquad (17e)$$

The above format is analogous to Equations (5) Chapter 2, of Reference 10. The corresponding eigenvalue problem of the homogeneous systems is:

$$(\lambda_k [A] + [B]) \{X_k\} = \{0\}; \tag{18a}$$

where, in this case,

$$[A] = [R] - \{C\} \{C\}^T / I_{22}. \tag{18b}$$

Software was developed to solve the above eigenvalue problem, and to calculate natural modes, frequencies, and damping factors (Figure 6).

2.7 Sample Calculations

For the nominal input parameters of Hermes (Tables 1-5), the software of section 2.6 yields the modal values given in Table 6. As discussed earlier, the nature of coupling in the system is such that symmetric results can be arrived at with the pitch program whereas antisymmetric modes are associated with roll/yaw. The frequencies essentially agree with those published in Reference 7 and other works and thus validates the software. No numerical or computational problems were experienced with the method.

Of significance in Table 6 is the fact that both frequency and damping ratio associated with the unconstrained, fundamental, out-of-plane, and antisymmetric mode of vibration in orbit are

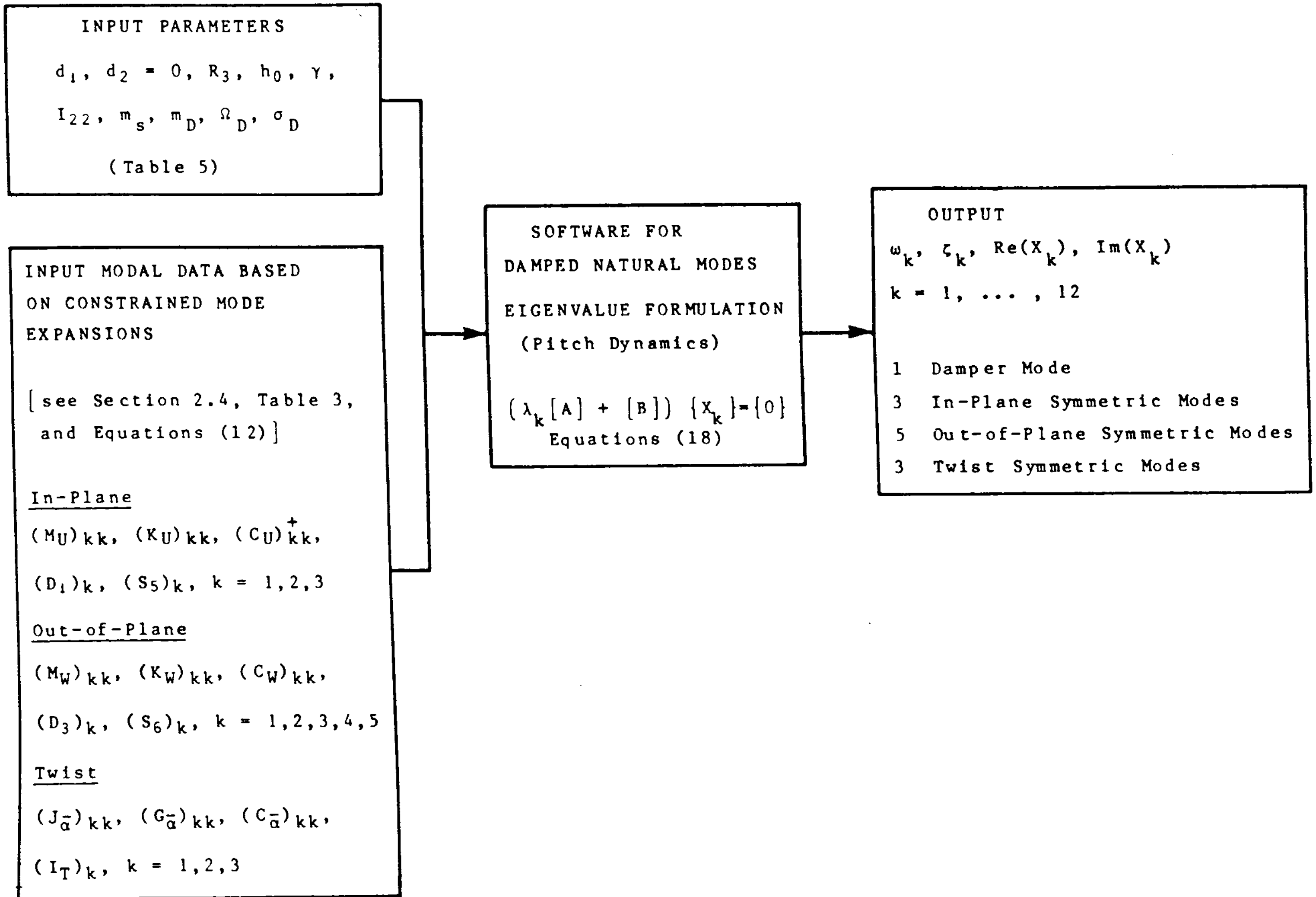

+Note, modal damping coefficients are related to damping ratios by Equations(5c)

FIGURE 6 Damped Natural Modes solution for pitch dynamics.

TABLE 5

NOMINAL INPUT PARAMETERS FOR SPACECRAFT HERMES+

PARAMETER	VALUE	UNITS
m_s	317.5	kg
I_{11}	1130	$kg.m^2$
I_{22}	1017	$kg.m^2$
I_{33}	1168	$kg.m^2$
I_{13}	0	$kg.m^2$
h_0	20	N.m.s.
γ	0	RAD
R_1	0	m
R_2	0.76	m
R_3	0	m
m_D	0.1145	kg
Ω_D	0.40	Hz
σ_D	0.004	--
d_1	-0.79	m
d_2	-0.29	m

\+ pertinent modal input characteristics for a single constrained array are as in Tables 3 and 4

TABLE 6

Unconstrained Modal Frequency and Damping Ratio Computed for Spacecraft Hermes Using Damped Natural Modes Theory

Mode Description	Mode Number, k	Frequency ω_k, Hz	Damping Ratio, ζ_k **
(a) Pitch Dynamics			
Out-of-plane, symmetric	1	0.149	0.0061
Out-of-plane, symmetric	2	0.506	0.0060
Out-of-plane, symmetric	3	0.957	0.0060
Out-of-plane, symmetric	4	2.489	0.0060
Out-of-plane, symmetric	5*	11.600	0.0060
In-plane, symmetric	1	0.324	0.0153
In-plane, symmetric	2	3.268	0.0150
In-plane, symmetric	3*	19.270	0.0150
Twist, symmetric	1	0.144	0.0909
Twist, symmetric	2	0.493	0.0909
Twist, symmetric	3*	0.925	0.0909
Damper	-	0.400	0.0040
(b) Roll/Yaw Dynamics			
Nutation	-	0.00277	4×10^{-8}
Damper	-	0.400	0.0043
Out-of-plane, Antisymmetric	1	0.444	0.0173
Out-of-plane, Antisymmetric	2	0.509	0.0066
Out-of-plane, Antisymmetric	3	0.970	0.0063
Out-of-plane, Antisymmetric	4	2.542	0.0060
Out-of-plane, Antisymmetric	5*	12.165	0.0060
In-plane, Antisymmetric	1	0.851	0.0393
In-plane, Antisymmetric	2	3.319	0.0155
In-plane, Antisymmetric	3*	19.300	0.0150

* Modes are not accurate, due to limitations of the Rayleigh-Ritz method used.

** Based on input damping ratios of 0.006 out-of-plane, 0.015 in-plane and 0.090 in twist for the constrained array substructure (Table 4) and a nominal value of 0.004 for the damper.

noticeably larger than those input values provided for the corresponding fundamental mode of the constrained array itself. This observation is important since it implies that one can expect, in certain cases, to measure both higher frequencies and higher damping ratios for structural modes of a spacecraft system in orbit as opposed to values measured at ground level for an individual constrained substructure. By way of explanation notice, for example, that array frequencies for the symmetric spacecraft lie quite near those for a single array under zero gravity, as shown in Table 3. Such an occurrence is anticipated for the symmetric case since vibrational momenta of the two arrays are equal in magnitude but opposite in direction, consequently satellite librations are not excited and the arrays behave essentially as constrained elements. The opposite is true during antisymmetric oscillation when the combined effect of vibration of the arrays is to force rotation of the central body. In this case the unconstrained system modal frequency can be significantly higher than that of the constrained substructure.

A simplified system consisting of roll motion together with a one mode approximation to antisymmetric out-of-plane array vibration is sufficient to demonstrate the nature of the interaction and is described in Appendix B. Effect of coupling is seen to be embodied in coefficient β [Equation (B.3f)] which is a function of spacecraft roll inertia, array generalized mass, and the coefficient associated with integral of the constrained mode shape. From Equation (B.3), unconstrained in-orbit frequency and damping ratio are $\omega = \beta\Omega$, $\zeta = \beta\sigma$ where, based on Hermes parameters, $\beta \simeq 3$ (fundamental array mode). That is, frequency and damping ratio for the fundamental antisymmetric and unconstrained out-of-plane modes are larger by a factor of three times that for the constrained array. The same degree of increase is not apparent for higher modes which can be attributed to their much smaller modal integral coefficients (S_k) as evident from Table 3 and Equations 12. Similarly, it can be established that, unless offset R_3 is significant, in-plane/out-of-plane unconstrained symmetric modes are effectively uncoupled from pitch since $S_5 \simeq S_6 \simeq 0$, implying $\beta \simeq 1$. Coupling with twist exists but would not be considered strong since, for this case, $\beta \simeq 1.04$.

This relationship between constrained and unconstrained modal properties is not a new concept.[31,32] The purpose here, however, is to emphasize the significance of this relationship when measuring damping ratios for space structures in-orbit.

Note, a degree of uncertainty is always present regarding actual shape of a given mode which, in turn, renders frequency less determinate. Equation (B.3f) enables one to estimate sensitivity of frequency to modal integral coefficient (S) as shown in Appendix B; see equation (B.7) and Table B-1. A difference of 10% in S results in an 80% change in frequency!

3.0 COMPARISON OF COMPUTED MODAL INFORMATION WITH FLIGHT-DERIVED RESULTS

3.1 Review and Update of Data Measured In-Orbit

This section summarizes and updates in-orbit measurements made of the dynamic properties of HERMES in the 3-axis stabilized state with a view to later comparison with calculated results.

The measurements of natural frequency and damping factor for the vibrational modes have been reported in References 3, 5 and 7. The measurements are derived from residual oscillations associated with array deployment and slewing, and from specially-implemented excitation by the thrusters (SPEX). Damping factors have been deduced from the decay envelope of free vibration (log decrement method) and from the sharpness given by the Fourier transform of the vibrational data. In preparing this report, both published and unpublished data were reviewed. Table 7 summarizes the results*. For most modes reported, the accelerometer data from which the results are deduced is of excellent quality, and the confidence level in the measurements is rated high. For the second

---

* Table 7 is consistent with published results except for the following: a mode at 0.46 Hz was reported to be a second antisymmetric in-plane mode in Ref. 7 , whereas herein it is identified as the second symmetric twist.

TABLE 7

Modal Frequency and Damping Ratio as Measured In-Orbit on Hermes[7]

Mode Number	γ RAD	Description of Mode	ω_k (Hz)	ζ_k
Nutation		Roll/Yaw	0.00293	0.00015
1	0	Out-of-Plane, Symmetric	0.150	0.030-0.038
1	0	Out-of-Plane, Antisymmetric	0.440	0.015-0.022
2	0	Out-of-Plane, Antisymmetric	0.500	0.007-0.008
1	0	In-Plane, Symmetric	0.300	0.030-0.039
1	0	In-Plane, Antisymmetric	0.820	0.012-0.016
1	$\pi/2$	In-Plane, Antisymmetric	0.980	
2	0	In-Plane, Antisymmetric	0.890	
1	0	Twist, Symmetric	0.130	0.080-0.090
2	0	Twist, Symmetric	0.460	

out-of-plane antisymmetric mode, the accelerometer data is of lower quality and the confidence level is rated medium.

Late in the mission, an in-orbit dynamics test was carried out to establish the characteristics of nutation in the 3-axis stabilized mode[8]. A nutation cone of one degree was initiated, the thrusters were inhibited, and the satellite was allowed to nutate without disturbance for 12 hours. Data from the tests are reproduced in Figure 7. The nutation period and damping factor were measured to be 341 seconds and 1.5×10^{-4}, respectively.

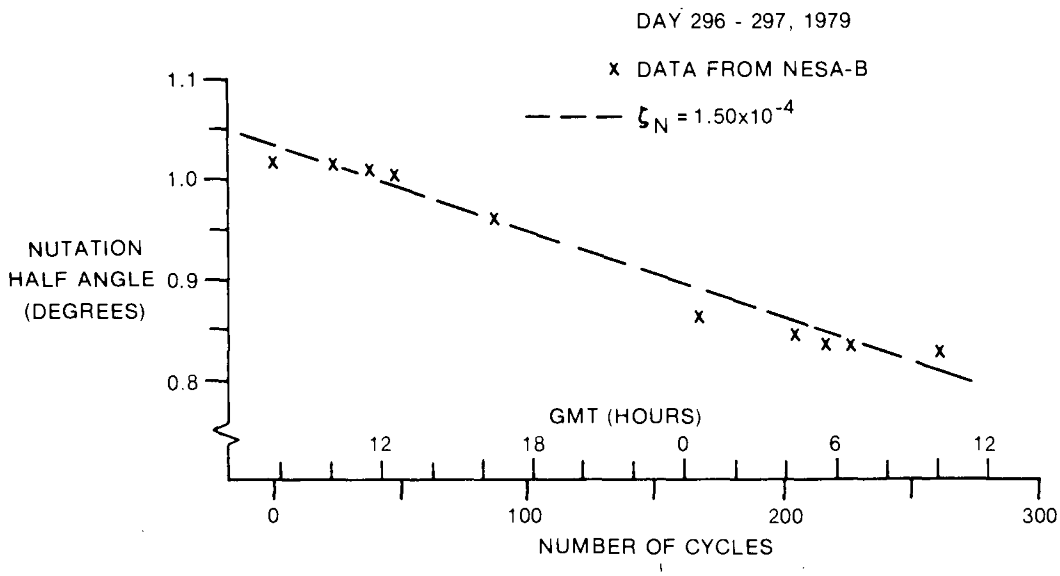

FIGURE 7 Measured orbital data reflecting nutational decay of Hermes with arrays fully deployed.

3.2 Measured Versus Calculated Frequencies

Comparison of the flight-measured and software-calculated frequencies of Tables 7 and 6 respectively shows that the numbers essentially agree. Thus the software operates correctly in this regard.

Also, the synthesized modal frequencies are consistent with those of the previously-reported work that uses modelling with no damping (i.e., Refs. 5 and 7). This is as expected, since damping is small.

It was also found in numerous computer runs, that the calculated frequencies were insensitive to changes in those damping factors that are typical of flight values (e.g. 0.05).

3.3 Influence of the Liquid Mercury Damper on System Damping

An objective in this section is to establish the degree to which damping factors measured in flight can be attributed to the damper. To isolate the effect of the damper, all other sources of damping are set equal to zero. Of the four damper input parameters(m_D, σ_D, Ω_D, and $\underline{d}$), only m_D and $\underline{d}$ are confidently known. The approach in this section is to vary Ω_D and σ_D in the computer program over a wide range in order to ascertain the theoretical limits of the damper's effect on spacecraft damping factors, and then to compare the calculated numbers with in-flight measurements.

Tables 8(a) and 8(b) summarize computer runs of the roll/yaw and pitch dynamics, respectively. The spacecraft's frequencies (ω's) do not change noticeably with changes in input damper parameters, and thus are not included in the Tables (i.e. assuming σ_D is not too much greater than 0.100, they remain essentially as given in Table 6).

From Table 8(a), it is seen that, when the damper is not near resonance (Ω_D = 0.00277 Hz), the damping factor of the nutational mode (ζ_N) is of order 10^{-12}, which is negligible compared to the flight-measured level of 1.5×10^{-4}. The variation in ζ_N with σ_D is shown in

Table 8(a)

Influence of Liquid Mercury Damper on Roll/Yaw Damping Characteristics

INPUT DAMPER PARAMETERS				OUTPUT MODAL DAMPING							
				NUTATION	IN-PLANE			OUT-OF-PLANE			DAMPER
m_D (kg)	Ω_D (Hz)	σ_D	d_2 (m)	ζ_N	ζ_1	ζ_2	ζ_3	ζ_1	ζ_2	ζ_3	ζ_D
0.1145	0.00277	10^{-5}	-0.29	5×10^{-6}							6×10^{-6}
0.1145	0.00277	10^{-4}	-0.29	5×10^{-5}							6×10^{-5}
0.1145	0.00277	10^{-3}	-0.29	5×10^{-4}							6×10^{-4}
0.1145	0.00277	2×10^{-3}	-0.29	9×10^{-4}							1×10^{-3}
0.1145	0.00277	5×10^{-3}	-0.29	5×10^{-4}							3×10^{-3}
0.1145	0.00277	10^{-2}	-0.29	2×10^{-4}							1×10^{-2}
0.1145	0.00277	10^{-1}	-0.29	2×10^{-5}							1×10^{-1}
0.1145	0.00277	9×10^{-1}	-0.29	2×10^{-6}							9×10^{-1}
0.1145	0.0015	0.006	-0.29	5×10^{-8}							6×10^{-3}
0.1145	0.0035	0.006	-0.29	2×10^{-7}							6×10^{-3}
0.1145	0.1500	0.006	-0.29	3×10^{-13}							6×10^{-3}
0.1145	0.0200	0.005	-0.29	1×10^{-10}							5×10^{-3}
0.1145	0.4000	0.100	-0.29	3×10^{-13}				8×10^{-5}	2×10^{-5}		1×10^{-1}
0.1145	0.4500	0.100	-0.29	2×10^{-13}				2×10^{-4}	4×10^{-5}		1×10^{-1}
0.1145	0.4500	0.500	-0.29	1×10^{-12}				3×10^{-5}	2×10^{-6}		6×10^{-1}
0.1145	0.5200	0.500	-0.29	3×10^{-13}				2×10^{-5}	2×10^{-6}		6×10^{-1}
0.4540	0.4500	0.100	-0.29	8×10^{-13}				6×10^{-4}	2×10^{-5}	4×10^{-6}	1×10^{-1}
0.4540	0.4500	0.100	-1.00	9×10^{-12}	1×10^{-6}			8×10^{-3}	2×10^{-4}	4×10^{-5}	1×10^{-1}
0.4540	0.4500	0.100	-2.00	4×10^{-11}	1×10^{-5}			3×10^{-2}	1×10^{-3}	4×10^{-4}	1×10^{-1}

Note: (1) $d_1 = 0$; $\omega_N = 0.00277$ Hz;
(2) input damping factors for the array substructure modes are zero;
(3) blank entries signify values of order less than 10^{-6}.

TABLE 8(b)

Influence of Liquid Mercury Damper on Pitch Damping Characteristics

INPUT DAMPER PARAMETERS				OUTPUT MODAL DAMPING			
m_D (kg)	Ω_D (Hz)	σ_D	d_1 (m)	DAMPER ζ_D	TWIST ζ_1	ζ_2	ζ_3
0.1145	0.15	0.001	-0.79	0.0010	2×10^{-6}	1×10^{-9}	3×10^{-10}
0.1145	0.15	0.010	-0.79	0.0100	2×10^{-5}	1×10^{-8}	3×10^{-9}
0.1145	0.15	0.100	-0.79	0.1000	2×10^{-5}	1×10^{-7}	3×10^{-8}
0.1145	0.324	0.010	-0.79	0.0100	2×10^{-8}	6×10^{-8}	7×10^{-9}
0.1145	0.400	0.001	-0.79	0.0010	7×10^{-10}	2×10^{-8}	1×10^{-9}
0.1145	0.400	0.010	-0.79	0.0100	7×10^{-9}	2×10^{-7}	1×10^{-8}
0.1145	0.400	0.100	-0.79	0.1001	7×10^{-8}	2×10^{-6}	1×10^{-7}
0.4540	0.400	0.100	-0.79	0.1003	3×10^{-7}	7×10^{-6}	4×10^{-7}
0.4540	0.400	0.100	-1.00	0.1004	4×10^{-7}	1×10^{-5}	7×10^{-7}
0.4540	0.400	0.100	-2.00	0.1018	2×10^{-6}	5×10^{-5}	3×10^{-6}

Note: (1) $d_2 = 0$;
(2) input damping factors for the array substructure modes are zero;
(3) output modal damping associated with in-plane, out-of-plane modes is of order less than 10^{-16} in all cases.

Figure 8 for the damper in resonance with satellite nutations; the maximum value is seen to be about 9×10^{-4}. Table 8 (a) also indicates that $\zeta_{1,OOP}$ changes linearly with m_D and probably quadratically with center of mass offset d_2. In Appendix A, approximate formulas are derived by the Method of Averaging (equivalent to the Energy Sink Method) which provide a functional relationship between ζ_N and the various damper parameters [see Equations (A.22), (A.23)]. As shown in Figure 8, such an approach yields excellent agreement with the

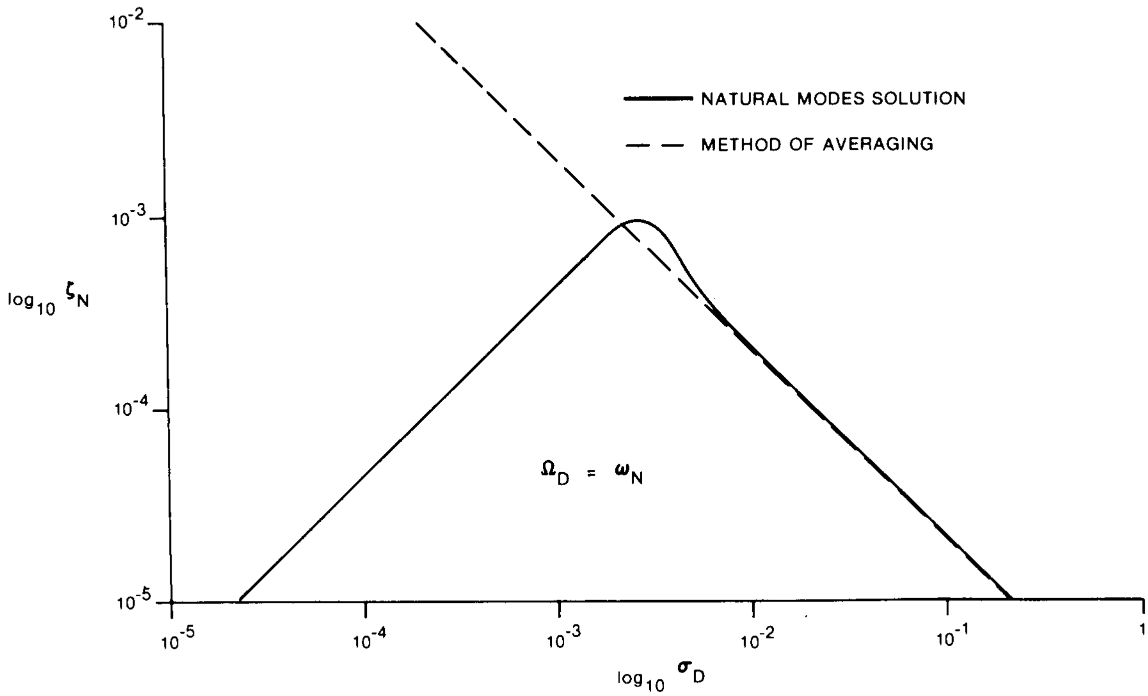

FIGURE 8 Nutational damping of Hermes for the case of a resonant damper.

Natural Modes calculations over the range $0.001 \leq \sigma_D \leq 0.100$ and thus confirms operation of the software. Also, according to Harris and Crede,[33] existence of a peak in distribution of the damping interaction effect can be expected in a system for which damping forces are comparable in magnitude to the effective stiffness forces . Hence, from Figure 8, it is concluded that the more exact Natural Modes approach is necessary in order to represent such a phenomenon. Away from resonance, the methods agree reasonably well as is shown in Appendix A where, at p_D = 0.020 Hz and ζ_D = 0.005, ζ_N becomes 3×10^{-11} and 10×10^{-11} when computed by Method of Averaging and the Natural Modes theory, respectively.

Table 8(a) reveals that when the damper frequency is near the nutation frequency, resulting ζ's of the antisymmetric vibrational modes are negligible $[0(<10^{-6})]$. Even when the damper is tuned near the first antisymmetric mode (0.444 Hz), the calculated damping factor is no higher than 10^{-4} (at the designed-for damper mass of 0.1145 kg and offset $d_2 = -0.29$m), which is still significantly less than the flight-measured 0.015 - 0.022.

Table 8(b) illustrates the influence of the damper on modes associated with pitch dynamics. Even with the damper tuned to be near resonance with the first twist mode, a maximum damping ratio of only 10^{-5} is found for the fundamental twist mode over the range $0.001 \leq \sigma_D \leq 0.100$, significantly less than the flight-measured value of 0.08 - 0.09. In-plane, out-of-plane modes are not affected as directly. For example, when the damper is tuned to the fundamental in-plane frequency, the maximum damping effect is again experienced by the first twist mode but to a much lesser degree than in the previous case. If the damper operates at the original design frequency (0.40 Hz), then it is the second mode in twist (0.49 Hz) which shows the largest damping ($\zeta_{2,TWIST} \approx 10^{-6}$ at $\sigma_D = 0.100$). As expected, an increase in m_D also augments the degree of damping interaction. However, the system is even more sensitive to offset of the damper from spacecraft center of mass. Note that in-plane, out-of-plane modal damping remains effectively uncoupled from the damper in all instances.

In summary, it can be concluded that: (a) the liquid mercury damper could have contributed the damping of the nutational mode, but to do so the fluid would have had to be excited to resonance by the nutations; (b) the damper did not contribute significantly to the damping factors of either the symmetric or antisymmetric vibrational modes; (c) the Method of Averaging validates operation of the Natural Modes software both at resonance and away from resonance. In addition, it identifies an analytic relation between the nutation damping and physical parameters of the spacecraft which has applicability over a significant range of frequencies (Ω_D) and damping (σ_D) of the damper subsystem.

3.4 Contribution of the Array Substructure to System Damping

The objective in this section is to establish the degree to which damping factors measured in flight can be attributed to damping sources in the arrays.

The array damping effect is isolated by setting σ_D of the damper equal to zero. Computer runs made using input damping values from the ground-based substructure test results of Table 4, and variations, are tabulated in Tables 9(a),9(b).

Table 9(a)

Contribution of Array Substructure to Damping of System Roll/Yaw Modes

ARRAY SUBSTRUCTURE INPUT DAMPING						OUTPUT MODAL DAMPING							
IN-PLANE			OUT-OF-PLANE			NUTATION	IN-PLANE			OUT-OF-PLANE			DAMPER
σ_1	σ_2	σ_3	σ_1	σ_2	σ_3	ζ_N	ζ_1	ζ_2	ζ_3	ζ_1	ζ_2	ζ_3	ζ_D
0.001	0.001	0.001				5×10^{-10}	2.6×10^{-3}	1×10^{-3}	1×10^{-3}	1×10^{-6}	1×10^{-7}	6×10^{-7}	1×10^{-9}
0.100	0.100	0.100				5×10^{-8}	2.7×10^{-1}	1.04×10^{-1}	1.01×10^{-1}	1×10^{-4}	9×10^{-6}	1×10^{-5}	1×10^{-7}
			0.001	0.001	0.001	6×10^{-9}	2×10^{-6}	7×10^{-10}	4×10^{-13}	2.9×10^{-3}	1.1×10^{-3}	1.1×10^{-3}	4×10^{-6}
			0.100	0.100	0.100	6×10^{-7}	1×10^{-4}	7×10^{-8}	4×10^{-11}	3.1×10^{-1}	1.04×10^{-1}	1.05×10^{-1}	4×10^{-5}
0.100	0.100	0.100	0.100	0.100	0.100	6×10^{-7}	2.7×10^{-1}	1.04×10^{-1}	3.0×10^{-1}	1.1×10^{-1}	1.04×10^{-1}	1.06×10^{-1}	4×10^{-5}
0.020	0.020	0.020				1×10^{-8}	5.2×10^{-2}	2.1×10^{-2}	2×10^{-2}	2×10^{-5}	2×10^{-6}	1×10^{-5}	2×10^{-8}
0.020	0.020	0.020	0.006	0.006	0.006	5×10^{-8}	5.2×10^{-2}	2.1×10^{-2}	2×10^{-2}	1.7×10^{-2}	6.6×10^{-3}	6.6×10^{-3}	2×10^{-5}
0.020			0.006	0.010		5×10^{-8}	5.2×10^{-2}	4×10^{-4}	6×10^{-6}	1.7×10^{-2}	1×10^{-2}	3×10^{-4}	2×10^{-4}
0.020	1.0	1.0	0.006	0.010	1.0	5×10^{-8}	5.3×10^{-2}	1	1	1.9×10^{-2}	1×10^{-2}	1	2×10^{-5}
0.020	0.020	0.020				6×10^{-9}	5.2×10^{-2}	2.1×10^{-2}	2×10^{-2}	2×10^{-5}	2×10^{-6}	1×10^{-5}	5×10^{-9}
1.0						3×10^{-7}	1	6×10^{-3}	3×10^{-4}	8×10^{-5}	4×10^{-6}	2×10^{-6}	2×10^{-7}
	1.0					1×10^{-12}	4×10^{-4}	1	1×10^{-5}	4×10^{-9}	1×10^{-9}	2×10^{-7}	1×10^{-12}
1.0	1.0	1.0				3×10^{-7}	1	0.98*	1	8×10^{-5}	4×10^{-6}	2×10^{-6}	2×10^{-7}

* $(\omega_2)_{IP}$ = 0.58 Hz for this case.

Note: (1) m_D = 0.1145 kg; $\sigma_D = 0$; $d_1 = 0$; $d_2 = -0.29$ m;
(2) blank entries are zero.

Table 9(b)

Contribution of Array Substructure to Damping of System Pitch Modes

INPUT PARAMETERS										OUTPUT MODAL DAMPING									
DAMPER	ARRAY SUBSTRUCTURE									DAMPER	TWIST			IN-PLANE			OUT-OF-PLANE		
	TWIST			IN-PLANE			OUT-OF-PLANE												
Ω_D (Hz)	σ_1	σ_2	σ_3	σ_1	σ_2	σ_3	σ_1	σ_2	σ_3	ζ_D	ζ_1	ζ_2	ζ_3	ζ_1	ζ_2	ζ_3	ζ_1	ζ_2	ζ_3
0.15	0.100	0.100	0.100							2×10^{-5}	0.1004	0.1001	0.1001						
0.15				0.100	0.100	0.100								0.1017	0.1001	0.1000			
0.15							0.001	0.001	0.001								0.1017	0.1001	0.1001
0.15	0.100	0.100	0.100	0.100	0.100	0.100	0.100	0.100	0.100	2×10^{-5}	0.1004	0.1001	0.1001	0.1017	0.1001	0.1001	0.1017	0.1001	0.1001
0.15	0.100	0.100	0.100	0.015	0.015	0.015	0.006	0.006	0.006	2×10^{-5}	0.1004	0.1001	0.1001	0.0153	0.0150	0.0150	0.0061	0.0060	0.0060
0.40	0.100	0.100	0.100	0.015	0.015	0.015	0.006	0.006	0.006	2×10^{-6}	0.1004	0.1601	0.1001	0.0153	0.0150	0.0150	0.0061	0.0060	0.0060
0.15	0.15			0.02			0.006	0.010		2×10^{-5}	0.1506	9×10^{-7}	2×10^{-7}	0.0204	1×10^{-7}	4×10^{-9}	0.0061	0.0100	9×10^{-8}
0.15	0.15	1.0	1.0	0.02	1.0	1.0	0.006	0.010	1.0	2×10^{-5}	0.1506	1	1	0.0204	1	1	0.0061	0.0100	1

Note: (1) $m_D = 0.1145$ kg; $\sigma_D=0$; $d_1 = -0.79$ m; $d_2 = 0$;

(2) blank entries signify zero or values of order less than 10^{-16}.

That effect which input array damping levels have on unconstrained system roll/yaw modal damping is demonstrated in Table 9(a) by varying the σ_k between 0.001 and 0.100. Should the array substructure have damping for the in-plane directions only, a nutation damping of $\zeta_N = 5 \times 10^{-10}$ to 5×10^{-8} results (i.e. ζ_N is proportional to $\sigma_{i,IN-PLANE}$). On the other hand, an initial damping associated with array out-of-plane motions only is seen to have an effect an order of magnitude greater which, however, is still not significant when compared with the measured level of $\zeta_N = 1.5 \times 10^{-4}$. The overall effect on ζ_N is no greater when in-plane, out-of-plane inputs are combined. Using input array damping ratios consistent with typical ground-based measurements still results in an insignificant effect on the nutation, that is $\zeta_N \simeq 5 \times 10^{-8}$.

Table 9(a) also provides information about the relationship between damping ratio for unconstrained antisymmetric modes (ζ_i) and the input damping associated with the constrained arrays (σ_i). Presence of a non-zero out-of-plane damping input gives rise to non-zero damping ratios for unconstrained in-plane modes and vice versa (i.e. if $\sigma_{k,IP} = 0.10$ or $\sigma_{k,OOP} = 0.10$, then $\zeta_{1,OOP} = 1 \times 10^{-4}$ or $\zeta_{1,IP} = 1 \times 10^{-4}$). Also, as expected, a change in damper frequency (Ω_D) affects only the unconstrained damper mode (ζ_D) and not vibrational or nutation damping ratio. Of interest, as well, is the influence which critical damping in one of the constrained substructure modes might have. For example, with a $\sigma = 1.0$ for the fundamental constrained in-plane mode, unconstrained in-plane damping ratios for the second and third modes of 0.006 and 0.0003 occur. An input of critically damped higher modes, however, does not result in significant output damping ratios. Note that, in general, it is the fundamental modes which undergo the greatest change (e.g. if $\sigma_{k,IP} = \sigma_{k,OOP} = 0.100$ then $\zeta_{1,IP} = 0.027$, $\zeta_{1,OOP} = 0.031$). This is consistent with the nature of the dynamic interaction occurring for this system as discussed in section 2.7 and is analogous to changes recorded in the frequencies (see tables 3, 6, 7 and Appendix B). Also, it is implied by such behaviour that the ζ's of spacecraft modes measured in-orbit are not sensitive to the input σ's of those higher order, and in most instances, unmeasured modes.

Table 9(b) provides data for modal damping of the symmetric modes. In all cases but one, damper frequency is set close to that of the fundamental twist mode in order to generate the maximum possible (resonant) effect. Input damping ratios for each class of array substructure modes (twist, in-plane, and out-of-plane) are first set separately to 0.100 and later are simultaneously set to this same level. Greatest effect is observed to be for the fundamental unconstrained modes ($\zeta_{1,TWIST} = 0.1004$, $\zeta_{1,IP} = \zeta_{1,OOP} = 0.1017$). No significant coupling in damping occurs between the different types of oscillation. Such findings are in line with the analysis outlined in section 2.7 and referred to above. Further, neither a shift in damper frequency nor the presence of a critically damped array input mode produces measurable changes of levels in the damping factors of the unconstrained symmetric modes.

3.5 Calculations Including Both the Liquid Mercury Damper and Array Damping in the Model

Computer runs made using nonzero input combinations for damper and array subsystem damping demonstrated that the effect of these two damping sources on unconstrained damping factor can be added in a linear fashion.

3.6 Measured Versus Calculated Unconstrained In-Orbit Damping Factors

The measured in-flight damping factors are compared to corresponding ones synthesized from the ground-test-derived substructures test results (Table 4) in Table 10 (Table 10 summarizes information from Tables 6 and 7). Based on a viscous damping model, agreement for first and second antisymmetric out-of-plane modes is reasonable (i.e. 0.017 versus 0.015 - 0.022 for $\zeta_{1,00P}$ and 0.0066 versus 0.007-0.008 for $\zeta_{2,00P}$). Good agreement exists as well for the fundamental symmetric twist (0.0907 versus 0.080-0.090). The

TABLE 10

Measured Versus Calculated Damping Factors

Mode Description	Calculated* ζ_k; σ_k from Ground-Based Data+		Calculated* ζ_k; σ_k derived from in orbit symmetric modes++		Flight Measured
	Viscous	Hysteretic	Viscous	Hysteretic	ζ_k (Table 3)
Nutation	4×10^{-8}	2×10^{-6}	2×10^{-7}	1×10^{-5}	1.5×10^{-4}
1st Symmetric, Out-of-Plane	0.0061	0.0061	0.0305	0.0305	0.030-0.038
1st Symmetric, In-Plane	0.0153	0.0163	0.0305	0.0325	0.030-0.039
1st Symmetric, Twist	0.0909	0.0977	0.0806	0.0868	0.080-0.090
1st Antisymmetric, Out-of-Plane	0.0173	0.0059	0.0872	0.0297	0.015-0.022
2nd Antisymmetric, Out-of-Plane	0.0066	0.0067	0.0328	0.0335	0.007-0.008
1st Antisymmetric, In-Plane	0.0393	0.0153	0.0788	0.0308	0.012-0.016

* Damping from Array Substructure Only, $\sigma_D = 0$.
\+ 0.015 in-plane, 0.006 out-of-plane and 0.090 in twist.
++ 0.030 in-plane, 0.030 out-of-plane and 0.080 in twist.

nutation, the first out-of-plane symmetric (0.006 versus 0.030 - 0.038), as well as first in-plane symmetric (0.015 versus 0.030 - 0.039) and antisymmetric (0.039 versus 0.012-0.016) modes, however, do not correlate well. Comparisons made using a hysteretic damping model are also given in Table 10, but there is a lack of good correlation with this method also. It should be borne in mind, however, that the lack of agreement is not necessarily due to shortcomings of the calculation process; for example, the input σ's have a high possibility of error due to the procedure used to convert from a one-g ground measurement to a zero-g in-orbit state.[3]

The question that naturally arises next is, 'is there any set of input σ's which leads to calculated ζ's that are consistent with flight data'. The input constrained modes are very similar to the flight-measured symmetric unconstrained modes (the spacecraft central body is heavy relative to the arrays and is essentially a fixed-base in orbit - see section 2.7), and thus it is logical to try, as the input σ's, the corresponding flight-measured symmetric ζ's. The runs corresponding to this concept are listed in Table 10 as well, for both a viscous and a hysteretic model. As would be expected, the ζ's for the symmetric modes match the flight data well. However no consistency exists when comparing nutational or antisymmetric modes.

One notes in Table 10 that the calculated ζ_N is significantly lower than the measured ζ_N. In Appendix A an approximate formula, derived by the Method of Averaging [Equation (A.15)], yields estimates of ζ_N which agree favourably with the more exact calculations of Table 10. Two conclusions may be drawn; either the array is not the source of damping causing the ζ_N, or the modelling of array damping ('hysteretic' or 'viscous') is basically in error.

3.7 Discussion and Overall Impressions

In the material presented in sections 3.3-3.6, it is evident that several of the computed ζ's do not correlate with measured ζ's to a completely satisfactory degree. The following impressions emerge as to possible reasons for the differences between computed and measured data:

(a) The liquid mercury damper, is not a main contributor to damping of vibrational modes. It can be expected that like calculations (not done) would also rule out the heatpipe. However, these devices could have contributed to the measured nutation damping, if they were excited at a resonant state.

(b) The argument that 'the mechanisms that caused the array damping measured in ground test are different than those occuring in orbit' would help explain discrepancies experienced in using ground-test-derived constrained mode input data, but this leaves unexplained discrepancies which persist when using constrained mode input data as derived from in-flight unconstrained symmetric modes. Consequently, this argument alone does not explain the lack of correlation.

(c) Two candidate explanations could explain the lack of agreement:

(i) The models put forth for array damping, namely viscous, or hysteretic, are inadequate. A different model could improve correlations (for example, if one proposed that damping forces are proportional to ω^{-2}, then correlations would be better in some cases).

(ii) There is a source(s) of damping which is unmodelled, such as friction in joints between solar array and body.

(d) The hydrazine fuel in the tanks is not believed to be the source alluded to in c(ii) above, firstly because the system was pressurized and did not allow sloshing or appreciable motion, and secondly there was no noticeable change in ζ's over the time period that the fuel depleted from its original 40 lb. to less than 10 lb.

4.0 CONCLUSIONS

This report demonstrates a method for calculation of system damping factors that is based on solving the 'general' eigenvalue problem for the motion equations, given component data as the base input information. The method is seen to be systematic and have no computational instabilities or procedural problems. Numerical experiments show that the method is not sensitive to errors in or omission of damping factors of the higher order modes of the substructure (which are generally not available from test data). The procedure herein avoids potential mathematical errors resulting from non-rigorous diagonalization of damping matrices that is involved in similar synthesis methods based on undamped modal theory.

The application to the Hermes data demonstrates the level of performance of the method. The synthesized modal damping factors differ relative to measured data by factors ranging from zero to five. All synthesized modal frequencies agree with flight measured data, and thus are consistent with previously reported works based on models with no damping. The damping source for the structural modes is structural damping of the solar array. The liquid mercury damper likely contributed to damping of the nutational mode.

Although the level of quantitative correlation between measured and sythesized damping factors is similar to that of the few earlier published works, it is somewhat disappointing. The shortcomings in correlation are believed to be due to inadequacies in the law chosen to model damping of the solar arrays, or possibly to omission of a major unidentified source of damping (such as friction between the substructures).

The method can be used for synthesizing damping for future spacecraft, provided that the potential shortcomings in accuracy are recognized and allowed for. It is believed that the method has the potential of being refined to a more reliable and accurate process, through development of tractable component models together with a wider variety of closely-controlled substructure-to-structure synthesis and laboratory exercises.

5.0 BIBLIOGRAPHY

1. Kana, D.D., and Huzar, S., "Synthesis of Shuttle Vehicle Damping Using Substructure Test Results," J. Spacecraft and Rockets, Vol. 10, Dec. 1973, pp. 790-797.

2. Hasselman, T.K., "Damping Synthesis from Substructure Tests," AIAA Journal, Vol. 13, October 1976, pp. 1409-1418.

3. Vigneron, F.R., "Ground-Test Derived and Flight Values of Damping for a Flexible Spacecraft," ESA-SP-117, Proc. Symposium on Dynamics and Control of Non-Rigid Spacecraft, Frascati, Italy, May 24-26, 1977, pp. 325-333.

4. Santini, P., Castellani, A., and Nappi, A., "An Introduction to the Problem of Dynamic Structural Damping," AGARD Report #663, January 1978.

5. Vigneron, F.R., "Dynamics, Control and Structural Flexibility Results From the Hermes Mission," in Astronautics for Peace and Human Progress, Pergamon Press, 1979, pp. 397-411.

6. Vigneron, F.R., and Hughes, P.C., "Structural Dynamics Modelling for Hermes - Modelling and Measurement," Hermes (The Communication Technology Satellite) Its Performance and Applications, Proceedings of the Royal Society of Canada, 20th Symposium, 1977, IBSNO - 920064-12-4.

7. Garg, S.C., Hughes, P.C., Millar, R.A., and Vigneron, F.R., "Flight Results on Structural Dynamics from Hermes," J. Spacecraft & Rockets, Vol. 16, No. 2, March-April 1979, pp. 81-87.

8. Vigneron, F.R., "Passive ACS Test - Results on Decay of Nutation with Time," Memo #CRC 7501-11, 30 October 1979, Internal Communication, Communications Research Centre, Ottawa, Canada (available from authors).

9. Vigneron, F.R., and Krag, W.E., "Optical Measurements and Attitude Motion of Hermes After Loss of Stabilization," AIAA-82-4256, J. of Guidance, Control, and Dynamics, Vol. 5, No. 5, Sept.-Oct. 1982, pp. 539-541.

10. Vigneron, F.R., "Natural Modes and Real Modal Variables for Flexible Spacecraft," Canada Dept. of Communications, CRC Report #1348, November 1981.

11. Vigneron, F.R., "Dynamics Equations in Discretized Form for Flexible Three-Axis Stabilized Communications Satellites," Canada Dept. of Communications, Tech. Memo #SMD-6 Sept. 1976.

12. Alfriend, Kyle T., "The Partially Filled Viscous Ring Damper," AIAA 11th Aerospace Sciences Meeting, Washington, D.C., Paper No. 73-143, January 10-12, 1973.

13. Abramson, Norman H., (Editor), "The Dynamic Behaviour of Liquids in Moving Containers," NASA, SP-106, 1966.

14. Ancher, L.J., et. al., "Study on Passive Nutation Dampers. Volume 1:Literature Survey and Analysis. Volume 2:Damper Selection and Dimensioning. Volume 3:Appendices," European Space Agency, Report #ESA CR (P) - 788, December 1975.

15. Dennett, R.H., "Parametric Studies Associated With Spin-Stabilised Flexible Spacecraft," ESA SP 117, Proc. Symposium on Dynamics and Control of Non-Rigid Spacecraft, Frascati, Italy, May 24-26, 1976, pp. 177-189.

16. Rogers, E.E., "A Mathematical Model for Predicting the Damping Time of a Mercury Damper," U.S. Naval Ordnance Test Station, Pasadena, Calif., Report IDP565, 1959.

17. Likins, P.W., "Effects of Energy Dissipation on the Free Body Motions of Spacecraft," NASA, Tech. Report No. 32-860, July 1, 1966.

18. McElvain, R.J., "ATS S/S Nutational Damper Predicted Performance - Unsymmetrical Vehicle Configuration," Hughes Aircraft Co., Interdepartmental Memo, #2223/1582, 15 September 1965.

19. "RFPNo. SPAR 135 Proposal for CTS Program Nutation Damper," Hughes Aircraft Co., Ref. No. 72(41) - 12883/C8075, Vol. I-A, 11 August 1972.

20. "Specific Design Changes Between Hughes Design Review Inventory HS333/0167 (TELSAT) and the CTS Nutation Damper," Hughes Aircraft Co., El Segundo, Calif., 7 May 1973.

21. Williams, D.D., "Torques and Attitude Sensing in Spin-Stabilized Synchronous Satellites," Torques and Attitude Sensing in Earth Satellites, S.F. Singer, Ed., Academic Press, New York, 1964, pp. 159-174.

22. Vigneron, F.R., Canada Dept. of Communications, Memo #CRC 6666-15-1 (ST) Program, 20 January 1976. Also follow up memo on 22 January 1976.

23. Cloutier, G.J., "Resonances of a Two-DOF System on a Spin-Stabilized Spacecraft," AIAA J., Vol. 14, No. 1, January 1976, pp. 107-109.

24. Cochran, J.E., Jr., and Thompson, J.A., "Nutation Dampers vs. Precession Dampers for Asymmetric Spacecraft," J. Guidance and Control, Vol. 3, No. 1, January-February, 1980, pp. 22-28.

25. Taylor, R.S., "A Spring-Mass Damper for a Spin-Stabilized Satellite," TRW Systems, Redondo Beach, California, Report EM 11-15, 1961.

26. Bishop, R.E.D., "The Treatment of Damping Forces in Vibration Theory," J. Royal Aeronautical Society, Vol. 59, November 1955, pp. 738-742.

27. Vigneron, F.R., "A Structural Dynamics Model for Flexible Solar Arrays, of the Communications Technology Satellite," Canada Dept. of Communications, CRC Report #1268, April 1975.

28. Zurawski, S.J., and Cloutier, R.E., "Computer Program for 'A Structural Dynamics Model For Flexible Solar Arrays of the Communications Technology Satellite'," Canada Dept. of Communications, CRC Tech. Memo #SMS-3, June 1975.

29. Sincarsin, G.B., and Hughes, P.C., "Dynamic Ground Testing of the Hermes (CTS) Development Model Solar Array: Theory and Experiment," Proc. of Symp. on Dynamics and Control of Large Flexible Spacecraft, Blacksburg, Virginia, June 13-15, 1977, pp. 75-86.

30. Hughes, P.C., "Modal Identities for Elastic Bodies, With Application to Vehicle Dynamics and Control," ASME J. of Applied Mechanics, Vol. 47, March 1980, pp. 177-184.

31. Lips, K.W., "Dynamics of a Large Class of Satellites With Deploying Flexible Appendages," Ph.D Thesis, University of British Columbia, August 1980, pp. 94-96.

32. Millar, R.A., and Vigneron, F.R., "Effect of Antisymmetric Array Bending Motion (Excited by Thruster Control Torques) on Satellite Attitude," Canada Dept. of Communications, Tech. Memo No. CRC 6666-9-8 (NSTL) PROGRAM, June 28, 1971, p. 3.

33. Harris, Cyril M. and Crede, Charles E., "Shock and Vibration Handbook," Second Edition, McGraw-Hill Inc., 1976, p. 37-6.

34. Thomson, William T., "Theory of Vibration With Applicaitons," Prentice-Hall Inc., 1972,

35. Vigneron, F.R., "Stability of a Dual-Spin Satellite with Two Dampers," J. Spacecraft and Rockets, Vol. 8 No. 4, April 1971, pp. 386 - 389.

APPENDIX A

FORMULAS FOR DAMPING OF SPACECRAFT NUTATIONAL MODE AS DERIVED BY THE METHOD OF AVERAGING

In this Appendix, certain subsets of Equations (7) through (11) are solved by the Method of Averaging. The background of this technique is discussed more fully in Reference 35 and works cited therein, and will not be described extensively here. The procedure leads to formulas which relate explicitly the damping factor of the nutational mode (ζ_N) with parameters of the array substructure or the nutation damper.

CONTRIBUTION FROM THE ARRAY SUBSYSTEM

Consider the special case where the nutation damper is absent. In order to demonstrate the main effect without unnecessary analytic complication, further specialize the model to include only one shape factor for out-of-plane vibration (e.g. the fundamental mode) and no in-plane motion. Note as well that no essential mechanisms are lost if γ is chosen equal to zero and $I_\perp$ is taken equal to I_{33}. Equations (7) and (8b) then assume the form:

$$I\,\dot{\omega}_1 + h_0\omega_3 - 2S\ddot{W} = 0; \qquad \text{(A.1a)}$$

$$I\,\dot{\omega}_3 - h_0\omega_1 = 0; \qquad \text{(A.1b)}$$

$$M\ddot{W} + C\dot{W} + KW - S\dot{\omega}_1 = 0. \qquad \text{(A.2)}$$

In the above equations, all quantities are scalars. ω_1, ω_3 can be transformed to two new variables, A and B, as follows:

$$\omega_1(t) = A(t)\cos p_N t + B(t)\sin p_N t \;; \qquad \text{(A.3a)}$$

$$\omega_3(t) = A(t)\sin p_N t - B(t)\cos p_N t \;; \qquad \text{(A.3b)}$$

where,

$$p_N = h_0/I \;. \qquad \text{(A.3c)}$$

Differentiating Equations (A.3) and substituting into (A.1) results in:

$$\dot{A}\cos p_N t + \dot{B}\sin p_N t = (2S/I)\ddot{W}; \qquad \text{(A.4a)}$$

$$\dot{A}\sin p_N t - \dot{B}\cos p_N t = 0 \;. \qquad \text{(A.4b)}$$

Appropriate multiplication by $\cos p_N t$, $\sin p_N t$ together with additions and subtractions permits Equation (A.4) to be rearranged into the form:

$$\dot{A} = (2S/I)\ddot{W}\cos p_N t \;; \qquad \text{(A.5a)}$$

$$\dot{B} = (2S/I)\ddot{W}\sin p_N t \;. \qquad \text{(A.5b)}$$

Applying Equations (A.3a), (A.5) to Equation (A.2) leads to the following vibration equation expressed in terms of the transformed nutation parameters:

$$\ddot{W} + 2\, p_\iota \zeta_\iota\, \dot{W} + p_\iota^2 W = F_0\ (-A \sin p_N t + B \cos p_N t)\ ; \quad (A.6)$$

where,

$$p_\iota^2 = K/[M(1 - \frac{2S^2}{MI})]; \quad (A.7a)$$

$$2\zeta_\iota p_\iota = C/[M\ (1 - \frac{2S^2}{MI})]; \quad (A.7b)$$

$$F_0 = h_0 S/[MI\ (1 - \frac{2S^2}{MI})]. \quad (A.7c)$$

Equations (A.5) and (A.6) are exact equivalents of Equations (A.1) and (A.2) with variables (ω_ι, ω_2) replaced by variables (A, B). Equations (A.5) and (A.6) are in a form amenable to solution by the formal method averaging.

By way of physical explanation, the equations indicate that there are two frequencies associated with the dynamics, p_N and p_ι. p_N is the nutational frequency of an equivalent rigid satellite, p_ι and ζ_ι are the well known first approximations to the unconstrained first out-of-plane modal frequency and damping factor. For Hermes p_N is much smaller than p_ι. During steady state nutation at frequency p_N (after transients of frequency p_ι have damped down.), A and B are approximately constant for 'long' periods of time so that the unconstrained deformation, W, is excited by the nutation at frequency p_N as per Equation (A.6).

Following procedures of the formal Method of Averaging, Equation (A.6) is first solved with A, B set equal to their averaged (essentially constant) values $\bar{A}$, $\bar{B}$ in order to obtain an 'averaged' steady state value for W:

$$W(t) = \frac{F_0}{p_\perp^2 D} \left[-\bar{A} \sin (p_N t - \phi_N) + \bar{B} \cos (p_N t - \phi_N) \right] ; \quad (A.8)$$

with,

$$D = \{ [1 - (p_N/p_\perp)^2]^2 + [2 \zeta_\perp (p_N/p_\perp)]^2 \}^{\frac{1}{2}} ; \quad (A.9a)$$

$$\sin\phi_N = 2(p_N/p_\perp) \zeta_\perp / D ; \quad (A.9b)$$

$$\cos\phi_N = [1 - (p_N/p_\perp)^2]/D . \quad (A.9c)$$

Response W(t) of Equation (A.8) is next to be substituted into Equation (A.5a) and this equation, in turn, is averaged over one period of nutation, thus resulting in a differential equation for long-term average behaviour of the nutation parameters A, B:

$$d\bar{A}/dt = a_{1\perp}\bar{A} - a_{2\perp}\bar{B} ; \quad (A.10a)$$

$$d\bar{B}/dt = a_{2\perp}\bar{A} + a_{1\perp}\bar{B} . \quad (A.10b)$$

where:

$$a_{1\perp} = - (p_N/p_\perp)^2 (SF_0/ID) \sin\phi_N ; \quad (A.11a)$$

$$a_{2\perp} = (p_N/p_\perp)^2 (SF_0/ID) \cos\phi_N . \quad (A.11b)$$

The latter coefficients can be rewritten using Equations (A.7c) and (A.9):

$$a_{1\perp} = -2p_N \left\{ \left(\frac{1}{2D^2}\right) \left(\frac{p_N}{p_\perp}\right)^3 \left(\frac{2S^2}{MI}\right) \left[\frac{1}{(1-2S^2/MI)}\right]\right\} \zeta_\perp \; ; \qquad \text{(A.12a)}$$

$$a_{2\perp} = \tfrac{1}{2}\left\{ \left(\frac{1}{D^2}\right) \left(\frac{p_N}{p_\perp}\right)^2 \left[1-\left(\frac{p_N}{p_\perp}\right)^2\right] \left(\frac{2S^2}{MI}\right) \left[\frac{1}{(1-2S^2/MI}\right]\right\} p_N \; . \qquad \text{(A.12b)}$$

Solution of Equations (A.10) take the form:

$$\bar{A}(t) = e^{a_{1\perp}t}\left(\bar{A}_0 \cos a_{2\perp}t - \bar{B}_0 \sin a_{2\perp}t\right) \; ; \qquad \text{(A.13a)}$$

$$\bar{B}(t) = e^{a_{1\perp}t}\left(\bar{A}_0 \sin a_{2\perp}t + \bar{B}_0 \cos a_{2\perp}t\right) \; ; \qquad \text{(A.13b)}$$

where $\bar{A}_0$, $\bar{B}_0$ represent initial averaged values. Equation (A.13) can be substituted into (A.3) to obtain the expression for $\omega_\perp(t)$:

$$\omega_\perp(t) = e^{a_{1\perp}t}\left[\bar{A}_0 \cos(p_N - a_{2\perp})t + \bar{B}_0 \sin(p_N - a_{2\perp})t\right] \; . \qquad \text{(A.14)}$$

A similar relation can be obtained for $\omega_3(t)$.

Equations (A.8), (A.14) constitute a 'first' approximation solution to the system dynamics [Equations (A.1), (A.2)] and can be expected to be valid provided the right hand sides of Equation (A.5) are 'small'. This is the case when $p_N \ll p_\perp$, as can be seen from Equations (A.5), (A.10) and (A.12a).

From Equation (A.14) it is deduced that the effective damping ratio of the nutation mode is related to $a_{1 1}$ through the relation;

$$a_{1 1} = 2\zeta_N (p_N - a_{2 1}) \quad .$$

When $p_N \ll p_1$, D is approximately unity, $(p_N - a_{2 1})$ equals ω_N and hence,

$$\zeta_N \simeq \tfrac{1}{2} \left(\frac{p_N}{p_1}\right)^3 \left(\frac{2S^2}{MI}\right) \left(\frac{1}{1-2S^2/MI}\right) \zeta_1 \quad . \tag{A.15}$$

Clearly, an identical relation can be derived for either the in-plane or any other well-separated modal frequency in which case p_1, M, S and ζ_1 would be replaced by their appropriate values. The resulting ζ_N is then the sum of the contributions as calculated from (A.15), for each mode.

Equation (A.15) is calculated with the initial assumption that the damping law for the array is 'viscous'. If a 'hysteretic' damping relationship were to be assumed at the out-set, then effectively the damping term of Equation (A.6) would be made inversely proportional to p_N. Carrying this through the algebra yields a final result:

$$\zeta_N^* = (p_1/p_N)\ \zeta_N \ ; \tag{A.16}$$

where, ζ_N^* denotes the damping coefficient based on a hysteretic damping model and ζ_N is representative of a viscous damping effect as per equation (A.15).

For the Hermes parameters; $2S^2/MI \simeq 0.888$; $p_N \simeq 0.00277$ Hz. For the out-of-plane mode, $p_\perp = 0.45$ Hz so that the resultant damping factors are:

$$\zeta_N \simeq 9.29 \times 10^{-7} \quad \zeta_{1,OOP} \; ; \tag{A.17a}$$

$$\zeta_N^* \simeq 1.51 \times 10^{-4} \quad \zeta_{1,OOP} \; . \tag{A.17b}$$

For in-plane deformation, with $p_\perp \simeq 0.85$;

$$\zeta_N \simeq (1.39 \times 10^{-7}) \; \zeta_{1,IP} \; ; \tag{A.18a}$$

$$\zeta_N^* \simeq (4.23 \times 10^{-5}) \; \zeta_{1,IP} \; . \tag{A.18b}$$

A $\zeta_{1,OOP}$ of the order 0.020 then results in a maximum ζ_N^*, ζ_N of about 3×10^{-6} and 2×10^{-8}, respectively.

CONTRIBUTION FROM THE LIQUID MERCURY DAMPER

To demonstrate this effect, consider the case where the arrays are rigid and offset $d_\perp = 0$. Then Equations (7a), (7b) and (11) become:

$$I\dot{\omega}_1 + h_0\omega_3 - md_2\ddot{x}_D = 0 \; ; \qquad \text{(A.19a)}$$

$$I\dot{\omega}_3 - h_0\omega_1 = 0 \; ; \qquad \text{(A.19b)}$$

$$m_D\ddot{x}_D + c_D\dot{x}_D + k_Dx_D - m_Dd_2\dot{\omega}_1 = 0 \; . \qquad \text{(A.20)}$$

The above are analogous to Equations (A.1), (A.2) when the correspondence is made between 2S, M, C, K and m_Dd_2, $m_D/2$, $c_D/2$, $k_D/2$ respectively.

In order to assess a maximum possible effect, consider the case where the nutation damper is excited at resonance. Then, for Equation (A.12):

$$p_N = p_1 ; \; D \simeq 2\zeta_1 ; \quad \zeta_1 = \zeta_D/2; \; [2S^2/MI] \ll 1 \; ;$$

hence,

$$a_{11} \simeq -\tfrac{1}{4}\left(\frac{m_Dd_2^2}{I}\right)\left(\frac{p_N}{\zeta_D}\right); \quad a_{21} \simeq 0 \quad . \qquad \text{(A.21)}$$

Consequently,

$$\zeta_N \simeq \tfrac{1}{4}\left(\frac{m_Dd_2^2}{I}\right)\left(\frac{1}{\zeta_D}\right) \quad . \qquad \text{(A.22)}$$

For Hermes, m_D = 0.1145 kg; d_2 = 0.287 m; $I \simeq 1145$ kg.m^2 (nominal). Based on an estimate of 0.005 for ζ_D, Equation (A.22) yields the result:

$\zeta_N \simeq 4.1 \times 10^{-4}$ (versus 4.6×10^{-4} from the Natural Modes Theory) .

Away from resonance, values are much smaller (typically 10^{-12}) since for this case it can be shown:

$$(\zeta_N)_{p_N \ll p_D} \simeq \tfrac{1}{4}\left(\frac{m_D d^2}{I^2}\right)^2 \left(\frac{p_N}{p_D}\right)^3 \zeta_D \ . \qquad (A.23)$$

With $p_D = 0.020$ Hz and $\zeta_D = 0.005$, Equation (23) gives a $\zeta_N = 3 \times 10^{-11}$.

APPENDIX B

SIMPLIFIED MODEL FOR UNCONSTRAINED DAMPING AND FREQUENCY

This Appendix derives simple first-order formulas for the unconstrained antisymmetric natural frequency and damping factor in terms of the constrained model parameters of the solar arrays. Also the sensitivity of the formulas to mode shape is illustrated.

Consider Equations (7a) and (8b). Specialize them for the case where the array is represented by one constrained mode, the liquid mercury damper and momentum wheel are absent, and γ equals zero. The resultant equations are:

$$I\ddot{x} - 2S\ddot{y} = 0; \qquad \text{(B.1a)}$$

$$m\ddot{y} + c\dot{y} + ky - S\ddot{x} = 0; \qquad \text{(B.1b)}$$

where,

$$\begin{aligned} \dot{x} &= \omega_\ell; & y &= W_a; \\ I &= I_{\ell\ell}; & S &= (S_3)_\ell; \\ m &= (M_W)_{\ell\ell}; & c &= (C_W)_{11} \\ k &= (K_W)_{\ell\ell}. & & \end{aligned} \qquad \text{(B.1c)}$$

Substituting (B.1a) into (B.1b) results in the following:

$$(m - 2S^2/I)\ddot{y} + c\dot{y} + ky = 0. \qquad \text{(B.2)}$$

Recognizing that,

$$\Omega^2 = k/m; \qquad \text{(B.3a)}$$

$$c/m = 2\sigma\Omega; \qquad \text{(B.3b)}$$

Equation (B.2) can be put in the form:

$$\ddot{y} + 2\zeta\omega\dot{y} + \omega^2 y = 0; \qquad \text{(B.3c)}$$

where ζ, the effective unconstrained damping ratio associated with vibration in orbit, is given by:

$$\zeta = \beta\sigma; \qquad \text{(B.3d)}$$

and ω, the effective unconstrained frequency of vibration in-orbit, is given by:

$$\omega = \beta\Omega. \qquad \text{(B.3e)}$$

In the above, β and K are given by:

$$\beta^2 = 1/(1 - \frac{2S^2}{mI}) = 1/(1-K); \qquad \text{(B.3f)}$$

$$K = 2S^2/mI. \qquad \text{(B.3g)}$$

For the Hermes fundamental out-of-plane mode (Tables 2-5),

$$
\begin{aligned}
I &= 1130\ \mathrm{kg.m^2};\\
m &= 2.33\ \mathrm{kg};\\
k &= 2.03\ \mathrm{N.m^{-1}};\\
\Omega &= 0.934\ \mathrm{rad.s^{-1}}\ (\simeq 0.15\ \mathrm{Hz});\\
(B_3)_\perp &= 30.4\ \mathrm{kg.m};\\
(D_3)_\perp &= 4.99\ \mathrm{kg};\\
R_2 &= 0.762\ \mathrm{m}.
\end{aligned}
$$

For this set of parameters:

$$
\begin{aligned}
S &= R_2 D_3 + B_3 = 34.2\ \mathrm{kg.m};\\
K &= 0.888;\\
\beta^2 &= 8.96;\\
\beta &\simeq 3.00.
\end{aligned}
$$

Consequently,

$$
\begin{aligned}
\sigma &= 0.006 \quad \text{yields} \quad \zeta = 0.018;\\
\Omega &= 0.15\ \mathrm{Hz} \quad \text{yields} \quad \omega = 0.45\ \mathrm{Hz}.
\end{aligned}
$$

Data in Table 3 implies relatively small values of S for modes other than the fundamental. Hence, according to Equation (B.3f), $\beta \simeq 1$ so that virtually no change occurs in the unconstrained ω, ζ of the higher modes.

Sensitivity to Substructure Mode Shape

Of interest is amount of error introduced in predicting unconstrained frequencies and damping in-orbit as a result of error in modal properties. Setting,

$$\beta^2 = 1/\alpha ; \tag{B.4a}$$

then, from (B.3f):

$$\partial\beta/\partial S = K/[S\alpha^{3/2}] ; \tag{B.4b}$$

$$\partial\zeta/\partial S = \sigma K/[S\alpha^{3/2}] . \tag{B.4c}$$

Consider a percentage change f in S corresponding to a change ΔS. That is,

$$\Delta S = (f/100)S. \tag{B.5}$$

Corresponding change over the initial unconstrained damping ratio ζ_0 is:

$$\zeta/\zeta_0 = 1 + \left(\frac{K}{1-K}\right)\left(\frac{f}{100}\right). \tag{B.6}$$

An identical relation holds for frequency:

$$\omega/\omega_0 = 1 + \left(\frac{K}{1-K}\right)\left(\frac{f}{100}\right). \tag{B.7}$$

For the Hermes array,

$$\frac{K}{100(1-K)} = 0.08.$$

The sensitivity of unconstrained damping and frequency to substructure modal integral coefficient (S) is illustrated in the following table:

	S = 0	S = 34 kg.m		
		f		
		0%	+ 1%	+ 10%
ζ	0.006 (σ)	0.018(ζ_0)	0.019	0.032
ω, Hz	0.15 (Ω)	0.450(ω_0)	0.486	0.810
$\Delta\zeta$, $\Delta\omega$	NA	0%	8%	80%

Note the dramatic effect associated with changes in the mode shape coefficients. A 10% change in value of S can cause 80% error in predicted damping ratio and frequency!

CRC DOCUMENT CONTROL DATA

1. **ORIGINATOR:** Department of Communications/Communications Research Centre

2. **DOCUMENT NO:** CRC Report No. 1365

3. **DOCUMENT DATE:** August 1984

4. **DOCUMENT TITLE:** Damping Synthesis for a Spacecraft using Substructure and Component Data

5. **AUTHOR(s):** K.W. Lips and F.R. Vigneron

6. **KEYWORDS:**
   (1) Spacecraft
   (2) Substructure
   (3) Synthesis

7. **SUBJECT CATEGORY (FIELD & GROUP: COSATI)**

   22 Space Technology

   22 02 Spacecraft

8. **ABSTRACT:** Refer to Page ii of this Report.

9. **CITATION:** ______

RP&DS Rev. 1973

DATE DUE
DATE DE RETOUR
